Testing Models of Cenozoic Exhumation in the Western Greater Caucasus

Stephen J. Vincent[1], Mark L. Somin[2], Andrew Carter[3], Giovanni Vezzoli[4], Matthew Fox[5] & Benoit Vautravers[1]

[1]CASP, West Building, Madingley Rise, Madingley Road, Cambridge, CB3 0UD, UK

[2]Schmidt Institute of Physics of the Earth, Laboratory of Tectonics and Geodynamics, Russian Academy of Sciences, 10 B. Gruzinskaya St., 123995 Moscow, Russia

[3]Department of Earth & Planetary Sciences, Birkbeck College, Malet Street, London WC1E 7HX, UK

[4]Dipartimento di Scienze dell'Ambiente e della Terra, Università di Milano-Bicocca, Piazza della Scienza 4, Milano, 20126 Italy

[5]Department of Earth Sciences, University College London, Gower Street, London, WC1E 6BT, UK

Corresponding author: Stephen Vincent (stephen.vincent@casp.org.uk)

Key points:

- There is a marked lateral change in the Cenozoic cooling history of the crystalline core of the western Greater Caucasus
- The region with young cooling ages (between Mt. Elbrus and Mt. Kazbek) coincides with an area of mantle-sourced Late Miocene and younger magmatism
- If driven by buoyancy forces, cooling must be partitioned over short wavelengths by lithospheric heterogeneities

Abstract

The Greater Caucasus form the northernmost deformation front of the Arabia-Eurasia collision zone. Earlier thermochronometric studies on the crystalline core of the western Greater Caucasus highlighted an abrupt along-strike increase in cooling ages to the west of Mt. Elbrus. Twenty-eight thermochronometric analyses conducted as part of this study confirm this pattern. Overall Cenozoic exhumation was restricted to less than 5-7 km, with slow to moderate punctuated Oligo-Miocene cooling. Cooling rates increased during the Late Miocene to Pliocene. These are most rapid east of Mt. Elbrus, where they probably increased later than farther west (at c. 5 Ma rather than 10-8 Ma). Differential cooling rates do not appear to be driven by lateral variations in tectonic shortening. The region undergoing rapid young cooling does coincide, however, with an area of mantle-sourced Late Miocene and younger magmatism. Thermal relaxation or overprinting is ruled out because geomorphic and modern sediment flux data mirror the thermochronometric trends. The buoyancy effects of demonstrable mantle upwelling are capable of causing the magnitude of exhumation-related cooling recorded in this study, but typically act over wavelengths of several 100 km. We suggest that lithospheric heterogeneities are responsible for modulating the shorter wavelength differences in exhumation rate documented here. These heterogeneities may include the continuation of the same structures responsible for the eastern margin of the Stavropol High to the north of the Caucasus, although further work is required. Similar abrupt variations in mantle-supported uplift and exhumation modulated by crustal structure may occur in other mountain belts worldwide.

Keywords: Russia, Georgia, Arabia-Eurasia collision, thermochronometry, fission track, dynamic topography, lithospheric heterogeneities

1 Introduction

The Greater Caucasus is Europe's highest mountain range. It marks the northern deformation front of the Arabia-Eurasia collision zone between the Black and Caspian seas, some 400-475 km north-northeast of its associated suture zone (the Bitlis-Zagros suture; Figure 1). During the Jurassic to Eocene, prior to Arabia collision, the northerly subduction of Neo-Tethys resulted in the southern leading edge of Eurasia being affected by various upper plate processes. These included volcanic arc formation along the eastern Pontides and southern Transcaucasus [Kazmin et al., 1986], accretion of the Anatolide-Tauride and South Armenia continental blocks [Rolland, 2017; Sosson et al., 2010], and the opening of the Black Sea, South Caspian and Greater Caucasus basins [Brunet et al., 2003; Nikishin et al., 2012; Vincent et al., 2016].

Relatively deep-water 'flysch' sediments deposited in the Jurassic to Eocene Greater Caucasus Basin crop out along the southern slope of the Greater Caucasus [Adamia et al., 1992; Saintot et al., 2006a; Vincent et al., 2016] (Figures 2 & 3). Thinner successions of contemporaneous shallower-water sediment overlie the now partially exhumed basement of its northern and southern flanks in its western sector [Vincent et al., 2016]. These are represented by the crystalline core of the range and the Dziruli Massif, respectively (Figure 3).

The Greater Caucasus Basin formed the tectonic dislocation that became the locus of later Greater Caucasus mountain building [Adamia et al., 2011; Mosar et al., 2010; Saintot et al., 2006a; Vincent et al., 2016]. The timing of Greater Caucasus Basin closure and the subsequent pattern of Cenozoic exhumation in the Greater Caucasus is debated.

There is evidence for Eocene compressional deformation in the western Greater Caucasus [Baskakova and Nikishin, 2018; Mikhailov et al., 1999; Saintot and Angelier, 2002; Saintot et al., 2006a; Tari et al., 2018]. According to Vincent et al. [2007, 2016], this culminated in the closure of the western sector of the Greater Caucasus Basin, subaerial rock uplift and the formation of the proto-western Greater Caucasus around the Eocene-Oligocene transition. They interpreted Oligo-Miocene sediments along the southern margin of the range to have been deposited in successor foreland basins as contemporaneous south-directed thrust sheets loaded the former southern shelf of the Greater Caucasus Basin.

Cowgill et al. [2016], building on the earlier work of Avdeev and Niemi [2011], instead proposed that the Greater Caucasus Basin remained open until the Pliocene. In their interpretation any evidence for Oligo-Miocene subaerial uplift is restricted to the northern margin of the basin and resulted from the northerly subduction of ‘oceanic basin’ crust beneath it. Furthermore, they interpreted Oligo-Miocene sediments on the southern side of the range to have been deposited within the relic oceanic basin and later thrust southward onto its southern margin during final basin closure. They inferred the timing of basin closure from an episode of c. 5 Ma cooling in the crystalline core of the western Greater Caucasus. This was modelled from thermochronometric data from samples collected between the Plio-Pleistocene volcanic peaks of Mt. Elbrus and Mt. Kazbek [Avdeev, 2011; Avdeev and Niemi, 2011] (Figure 2).

Cowgill et al. [2016] proposed that c. 5 Ma Greater Caucasus Basin closure was the trigger for a deceleration of plate convergence and tectonic reorganization across the Arabia-

Eurasia collision zone. Vincent et al. [2007], instead, related basin closure around the Eocene-Oligocene transition to the far-field effects of initial Arabia-Eurasia collision, with this process being unrelated to later Arabia-Eurasia reorganization. Further details of these contrasting hypotheses can be found in the papers cited above and the ensuing correspondence [Cowgill et al., 2018; Vincent et al., 2018].

Given the geodynamic significance attached to the cooling history of the western Greater Caucasus as modelled by Avdeev and Niemi [2011], the current authors carried out apatite and zircon fission track (AFT, ZFT) and apatite (U-Th)/He (AHe) analyses on 21 bedrock and colluvial / fluvial medium- to high-grade metamorphic samples between 40.8°E and 43.1°E on either side of Mt. Elbrus (Table 1; Figure 2). Colluvial / fluvial samples were collected immediately downstream of actively eroding areas and were transported less than 8 km from their host outcrops. An AHe analysis was also carried out on a sample originally collected for the study of Vincent et al. (2011). These analyses are presented here and combined with new fluvial geomorphic and existing thermochronometric, geologic and geomorphic data to provide new insights into the Oligocene to recent cooling history of the western Greater Caucasus. In particular, we test: (1) whether the 5 Ma cooling phase identified by Avdeev and Niemi [2011] can be reproduced and, if so, how widespread it is; (2) whether a westerly increase in AFT cooling ages identified by Král and Gurbanov [1996] is replicated and, if so; (3) whether it is reflected in other uplift and exhumation proxies. We then go onto discuss what these observations may mean in terms of the wider geodynamic evolution of the region and their applicability to other mountain belts worldwide.

Although the focus of this study is the Cenozoic exhumation history of the western Greater Caucasus, exhumation data from the eastern Greater are briefly introduced and placed in their wider context in the discussion (section 8.3). Ultimately, however, it is unclear how relevant these data are to the region farther west, given the limited nature of this data set and the marked difference in the present-day geodynamics of the two sectors of the range (see below).

2 Geodynamic Setting

Instrumentally-recorded earthquake and GPS-derived velocity data indicate that there are large-scale lateral variations in the present-day dynamics of the Caucasus region (Figure 1). Large-magnitude seismicity (M>4.5) is concentrated around and to the east of Mt. Kazbek, with deep earthquakes north of the Caucasus and in the central Caspian indicating that the Transcaucasus and South Caspian Basin are being underthrust or subducted northward under the eastern Greater Caucasus and Apsheron Sill [Allen et al., 2002; Jackson, 1992; Jackson et al., 2002; Mellors et al., 2012; Mumladze et al., 2015].

GPS-derived convergence rates between the Transcaucasus [*sensu* Adamia et al., 1992], north of the Sevan-Akera suture zone, and the southern part of the eastern Greater Caucasus increase towards the east (Figures 1 & 4). Geologic, geomorphic and seismic data demonstrate that this active shortening is taken up on both the northern and southern flanks of the eastern Greater Caucasus [Allen et al., 2004; Forte et al., 2014, 2010; Mosar et al., 2010; Philip et al., 1989; Sobornov, 1994]. The western boundary of this geodynamically-active region is marked by the Northeast Anatolian fault zone, along which a series of earthquakes with sinistral fault solutions have been recorded (Figure 1) [Copley and Jackson, 2006; Jackson, 1992; Philip et al., 1989]. However, there is no evidence that this structure continues into the upper plate [cf. Philip et al., 1989]. Seismicity in the western Greater

Caucasus is restricted to above ~33 km (Figure 1). Mumladze et al. [2015] inferred this to be due to break-off of the equivalent slab farther east. Van der Meer et al. [2018] subsequently identified a positive velocity anomaly beneath the western Greater Caucasus at ~350-650 km depth that they attributed to this detached slab.

GPS-derived velocities in the central and northern parts of the western Greater Caucasus are negligible relative to Eurasia (Figure 1); geodynamic models typically group the Pontides, Eastern Black Sea, western Greater Caucasus and Eurasia together (Figure 4) [Reilinger et al., 2006]. Orogen-perpendicular convergence rates between the Pontides and Adjara-Trialet Belt (on the southern and eastern margins of the Eastern Black Sea) and the western Greater Caucasus are around 2-3 mm a^{-1}. Shortening is taken up within the southern part of the western Greater Caucasus (Figure 1). This is best constrained to the north of the Dziruli Massif between the Racha-Lechkumi and Utsera faults (see Figures 2 & 3 for locations) [Fuenzalida et al., 1997; Sokhadze et al., 2018; Triep et al., 1995]. It is in this region that the Racha earthquake, the largest instrumentally recorded earthquake in the Caucasus (Ms=7.0) was recorded. Seismic source studies indicate that the Racha earthquake was the result of reverse slip on a moderately-inclined (~30°) north-dipping fault, with aftershocks located at depths of ~3-13 km [Fuenzalida et al., 1997; Triep et al., 1995] (Figure 3). We interpret it to result from the southward transport of the Mesozoic fill of the Greater Caucasus Basin over the basement (Dziruli Massif) and cover of the Transcaucasus on the Racha-Lechkumi fault (Figure 3).

Whilst GPS and seismicity data indicate that the western Greater Caucasus is geodynamically less active than farther east, it is at the eastern end of the western Greater Caucasus that earlier thermochronometric studies have identified a region of rapid cooling and presumed exhumation that is the focus of this study [Avdeev and Niemi, 2011; Král and Gurbanov, 1996; Vincent et al., 2011]. This region also forms the main site of Late Miocene to Quaternary magmatism within the Greater Caucasus [Chernyshev et al., 2014; Gazis et al., 1995; Hess et al., 1993; Lebedev et al., 2009a, 2009b, 2011b; Lebedev and Vashakidze, 2014; Tutberidze, 2012]. It also includes some of its highest local relief [Forte et al., 2016] and highest elevations, and, as mentioned above, is the site of its largest instrumentally recorded earthquake [Triep et al., 1995] (Figure 2).

Four sectors of the western Greater Caucasus are defined in this study to help with its characterization; these are termed northwest, northeast, southeast and southwest and are marked by blue dashed lines on Figure 2. In a north-south direction, these sectors are defined by the range's drainage divide. The majority of the crystalline core of the range occurs on the northern side of this boundary. In an east-west direction, the sectors are divided by a boundary that runs through Mt. Elbrus coincident with the major change in cooling ages identified in earlier fission track data. To the south of the drainage divide this boundary runs between the catchment of the Inguri River to the east and the Galisga and Kodori rivers to the west. North of the drainage divide this boundary is defined by the influence of the Stavropol High. Rivers such as the Kuma that drain eastward into the Caspian Sea occur to the east of the boundary and rivers such as the Kuban that drain westward into the Sea of Azov occur to its west (Figure 2).

3 Previous Thermochronometric Studies

Three major fission track studies have been carried out in the western Greater Caucasus. Early work by Král and Gurbanov [1996] was carried out prior to fundamental advances in FT methodology and is therefore of uncertain reliability. Their work would appear to show a spatial trend in AFT cooling ages (Figures 5a & 6); in the north-eastern sector of the range, to the east of Mt. Elbrus, most ages cluster between 4-7 Ma, whilst in the north-western sector, to the west of Mt. Elbrus, AFT ages get progressively older, implying a decrease in exhumation rate in this direction.

Vincent et al. [2011] documented both AFT bedrock and detrital ages. They derived bedrock ages of 28±2 Ma or older within the crystalline core of the north-western part of the range (Figures 5a & 6). These were similar to, or older than, those obtained by Král and Gurbanov [1996] from the same region. Thermal modelling of a number of these samples identified cooling from the Oligocene, with a possible acceleration in rates in the Miocene. Detrital AFT time lags (the difference between cooling and depositional ages) recorded by Vincent et al. [2011] were typically large (>80 Ma). Some samples from the southern sectors of the range, however, yielded time lags of as little as 10 Ma implying Oligocene and Miocene average cooling rates in their northerly sediment source regions of 10°C Ma^{-1}. Together these results were interpreted to indicate heterogeneous, slow to moderate, punctuated Oligo-Miocene cooling in the northern sectors of the range.

Vincent et al. [2011] also reported a metasedimentary bedrock sample from the south-eastern sector of the western Greater Caucasus in west Georgia with an AFT cooling age of 2.5±0.6 Ma (Figures 5a & 6). With advection taken into account, they equated this to a relatively high exhumation rate of ~0.9 km Ma^{-1} (calculated using the AGE2EDOT program [Ehlers et al., 2005], with a 40°C km^{-1} geothermal gradient and a 10°C surface temperature). Lacking thermochronometric data from the crystalline core of the north-eastern sector of the western Greater Caucasus, Vincent et al. [2011] postulated that this exhumation event might either reflect the inversion of the former sedimentary fill of the Greater Caucasus Basin, south of the crystalline core of the range (their model 1), or that it might also involve the crystalline core of the range, but only to the east of Mt. Elbrus as suggested by the data of Král and Gurbanov [1996] (their model 2; Figure 7).

Avdeev and Niemi [2011] plugged the data gap of Vincent et al. [2011] by reporting AFT cooling ages to the east of Mt. Elbrus, in the north-eastern sector of the range. These range typically between 5-8 Ma, helping to validate the analysis of Král and Gurbanov [1996] and supporting model 2 of Vincent et al. [2011] (Figures 5a, 6 & 7). They modelled Oligo-Miocene cooling rates of ~4°C Ma^{-1}, using unreported fission track density and length distributions, followed by an increase to ~25°C Ma^{-1} at around 5 Ma; an event not evident in the Vincent et al. [2011] data set farther west.

Avdeev and Niemi [2011] also conducted AHe analysis. Although they reported average corrected cooling ages, all but a single sample (B3) show significant overdispersion (>25%) within sample replicates, so that the meaning of their average ages is unclear. Sample B3 yielded an average corrected AHe age that is older than its AFT central age. This is unlikely to be due to radiation damage effects as the ages are young and the U/Th concentrations are not especially high. As a consequence, the AHe dataset of Avdeev and Niemi [2011] have not been incorporated into this study. Individual corrected AHe grain ages ranged between 0.7 Ma and 22.9 Ma, with the majority being younger than 5 Ma [Avdeev, 2011].

Palaeozoic to Mesozoic ZFT cooling ages reported by both Vincent *et al*. [2011] and Avdeev and Niemi [2011] (Figures 5c & 6) imply that the overall amount of Cenozoic exhumation anywhere in the western Greater Caucasus is less than 5-7 km. This is based on a ZFT closure temperature of 210-220°C, a 10°C surface temperature and a static geothermal gradient of 30-40°C km^{-1}.

4 New Thermochronometric Analyses

We obtained 5 AHe, 19 AFT and 4 ZFT analyses in order to better constrain the cooling/exhumation history of the western Greater Caucasus. Samples were collected from both bedrock and colluvial / fluvial medium- to high-grade metamorphic rocks from the crystalline core of the range. Sampling was carried out on either side of Mt. Elbrus, north of the drainage divide. The sampling strategy was designed to generate data that overlapped spatially with the previous data sets. We were unable to sample in the Republic of Abkhazia, in the south-western sector of the western Greater Caucasus. It has therefore not been possible to test whether the high rates of exhumation identified by Vincent et al. [2011] in the south-eastern sector of the range in west Georgia, and interpreted to result from the inversion of the Greater Caucasus Basin, also occur farther to the west.

The thermochronometric analyses were carried out by the London Geochronology Centre based at University College London, UK. Full analytical details can be found in the supplementary data section. The FT results are presented in Table 2 and the AHe results in Table 3. Thermal histories were inferred using the program QTQt [Gallagher, 2012], which is based on a Bayesian transdimensional approach to data inversion. Model outputs are an ensemble of accepted thermal histories that approximate the posterior probability that the sample was at a specific temperature at a given time. This ensemble can be simplified to an expected model (a mean thermal history model weighted by the posterior probability of each individual thermal history) and associated 95% credible intervals that provide a measure of uncertainty.

4.1 Apatite Fission Track Results

There are two main AFT cooling age groupings apparent in our data, one between 2.4±0.5 Ma and 8.1±1.4 Ma, and the other between 18.2±2.2 Ma and 27.6±7.7 Ma (Table 2; Figure 6). Twelve samples have AFT cooling ages in the 2.4±0.5 Ma to 8.1±1.4 Ma age group. Eleven of these were collected from around or to the east of Mt. Elbrus in the north-eastern sector of the western Greater Caucasus (Figures 5b & 6). They have similar cooling ages to samples reported by earlier works from this region (Figures 5a & 6) and would suggest relatively rapid Late Miocene and younger exhumation. Sample MS_078_1 also falls into this age group (7.7±0.8 Ma), but occurs 100 km to the west of Mt. Elbrus at the southern margin of its crystalline core close to the Main Caucasus Thrust (Figures 5b & 6). It is the youngest AFT cooling age reported so far from the north-western sector of the western Greater Caucasus.

The second group comprises five samples with age ranges between 18.2±2.2 Ma and 27.7±7.7 Ma. Two additional samples have ages of 46.1±6.9 Ma and 48.2±2.5 Ma (Table 2). All of these samples occur in the north-western sector of the western Greater Caucasus, to the west of Mt. Elbrus (Figures 5b & 6), and would suggest much lower or punctuated exhumation rates. Ages are similar to those from the same region reported by Vincent *et al*. [2011] and to the majority of those reported by Král and Gurbanov [1996] (who also documented six samples with 12-16 Ma ages; Figure 5a).

There are no clear trends in AFT cooling age across the range in either its north-eastern or north-western sectors (Figure 8). The single cooling age reported by Vincent et al. [2011] in the south-western sector is as young or younger than those reliable ages to the north

(Figure 8b). This would suggest cooling is not focussed in the immediate hangingwall of the Main Caucasus Thrust and that, east of Mt. Elbrus, areas to its north and south may be cooling at approximately similar rates [model 2 of Vincent et al., 2011].

Due to the generally young ages and / or low uranium contents there are few track length data available for thermal history modelling (see below). This is not an issue for samples with young cooling ages as their ages can only signify rapid recent cooling.

4.2 Apatite (U-Th)/He (AHe) Results

We also carried out AHe analysis on five AFT samples from the north-western sector of the study area. Two samples, with low dispersion and similar grain sizes, yield average raw AHe ages of 10.0±1.7 Ma and 15.4±1.2 Ma (Table 3; Figures 5c & 6). Individual raw grain ages from two of the other samples are broadly consistent with these ages (Table 3). When paired with their AFT ages (46.1±6.9 Ma and 48.2±2.5 Ma, respectively), the former samples record upper crustal cooling of ~50°C during the Eocene to Miocene followed by a further ~50°C from then on. The fifth sample has a 4.2±0.5 Ma average raw age (Table 3). When paired with its 26.3±5.2 Ma AFT age, this would suggest a younger phase of cooling during the Late Oligocene to Early Pliocene followed by very rapid cooling from then on.

Figure 9 shows examples of individual sample thermal history models based on the AFT and AHe data. A common feature of these models is that cooling rates were modest prior to 10-8 Ma after which some models show a marked acceleration in cooling. Samples that do not show the recent increase in cooling were already at shallow crustal levels where temperatures were below the sensitivity of the AHe system, e.g. sample MS_002_51. This broadly mirrors the earlier thermal modelling of AFT only samples from west of Mt. Elbrus by Vincent et al. [2011] that identified a Miocene (c. <15 Ma) increase in cooling. In section 5 we model all of the apatite data to gain a regional rather than site specific perspective.

4.3 Zircon fission Track Results

Our ZFT analyses yield a wide variety of cooling ages (Table 2). Sample MS_015_1, from immediately south of Mt. Elbrus, yields the oldest age (231.6±17.2 Ma). This is similar to a range of ZFT samples recorded by Vincent et al. [2011] and Avdeev and Niemi [2011] from along the length of the northern part of the range that have Permo-Triassic ages between 223.2±18.0 Ma and 293.4±12.4 Ma (Figures 5d & 6). Samples MS_092_1 and MS_093_1, from the north-eastern part of the range, yield younger, Early Cretaceous cooling ages (120.3±8.4 Ma and 117.6±6.0 Ma, respectively). These cooling ages are similar to that obtained from sample WG137/1 (139.6±6.5 Ma) from the south-eastern part of the range that yielded the youngest AFT age identified in the study of Vincent et al. [2011] (Figure 5d). The Mesozoic ZFT cooling ages determined in this study again limit the overall amount of Cenozoic exhumation within the core of the Caucasus to less than 5-7 km.

Sample MS_004_3 from close to the Eldzhurtinskiy granite yielded 1.4±0.2 Ma AFT and 1.7±0.2 Ma ZFT cooling ages (Figure 5). These are consistent with the very young emplacement age of this pluton [c. 2.5 Ma; Hess et al., 1993] and, because of advection and the perturbation of the thermal structure of the upper crust, cannot be used to accurately determine exhumation rates (see section 6).

5 Inverse Modelling of the Thermochronometric Data for Exhumation Rates

In order to highlight the spatial and temporal trends in the thermochronometric data from this and earlier studies, we use a formal linear inverse method [Fox et al., 2014]. This approach has several advantages over simply interpolating between thermochronometric ages or time averaged exhumation rates. First, ages vary as a function of elevation and this complicates and potentially masks spatial trends when interpolating between ages. Second, it allows us to incorporate data from multiple thermochronometric systems. Third, it allows trends to be compared over coherent time intervals, as opposed to inferring exhumation rates from individual ages that are averaged over age-defined intervals. This also ensures that ages obtained with different systems from the same sample have a consistent exhumation rate history. Fourth, it accounts for an evolving thermal field below complex topography by decomposing the 4D thermal field into transient 1D thermal models that are consistent with exhumation rates and temperature perturbations about 1D thermal models due to surface temperature perturbations caused by modern topography.

As is required when interpolating between ages or time-averaged exhumation rates, several parameters must be specified. These include spatial smoothness constraints, regularization terms to account for data noise, exhumation history discretization and a thermal model. We discretize the exhumation rate history into time steps that are specified based on various global and regional (Paratethyan) unit boundaries (as set out in the caption to Figure 10). After running a number of sensitivity tests (Figure S1), we adopted a spatial correlation length scale of 25 km to provide smooth models that highlight regional trends. An overestimated correlation length scale parameter increases temporal resolution at the expense of spatial resolution, potentially leading to incorrect accelerations or decelerations depending on the locations of ages in space and time and the prior mean exhumation rate.

Alternatively, an underestimated value reduces the temporal resolution and changes in exhumation rate through time cannot be recovered [Fox et al., 2014; Schildgen et al., 2018]. A thermal model is used that results in present day geothermal gradients of up to 38°C km^{-1} for the most rapidly exhuming areas. This is similar to the geothermal gradient estimate of Vincent et al. [2011] (40°C km^{-1}) for the same region. Other parameters include an initial geothermal gradient of 26°C km^{-1} and a corresponding basal heat flow lower boundary condition at 100 km depth, an upper boundary condition at 0 km and a fixed surface temperature of ~4°C at ~1800 m asl. Perturbations around this 1D thermal model are predicted using the modern topography extracted from the global 30 arc-second GEBCO database [Weatherall et al., 2015]. The model does not account for changes in topography through time but given that the young AHe data are most sensitive to topography, the modern topography is better than assuming no topographic perturbation. For the purposes of focusing on the most recent cooling, the model starts at 33.9 Ma, when the western Greater Caucasus initially emerged above sea level [Vincent et al., 2007]. A prior mean exhumation rate of 0.4 km Ma^{-1} was adopted. This represents a preferred value in the absence of any effective data for the duration of the model. Exhumation rates will deviate from this prior value as effective data are incorporated into the model to derive the posterior rates. For example, the old zircon fission track ages will lead to a decrease in rates between the prior and posterior models. A prior standard deviation of 0.1 km Ma^{-1} represents the expected variation about the mean value. The variability in the final solution is determined by the spatial and temporal distribution of the data, the data uncertainties, the correlation length scale parameter and finally, the prior standard deviation, modified to yield reasonable results. These results are simply used to highlight regional trends in the data and we do not attempt to determine a unique solution to this inverse problem. For an analysis of the influence of these parameters on the final results, please see Fox et al. [2016] or Ballato et al. [2015].

Figure 10 shows the results of the inversion from which we infer variations in regional exhumation rates in space and time. The recent time steps show the predicted exhumation rates, the resolution value and the data that fall within each time interval. The resolution value equals 1 where the data constrain the exhumation rate independently of the prior rate and rates in other time steps, while values less than 1 highlight areas where the model is less well resolved. For example, if 4 time intervals are required to explain a single isolated age, resolution values of less than 0.25 would be expected in each time interval, because the exhumation rate in each time interval depends on the exhumation rates in the other time intervals [Fox et al., 2014]. It is therefore not clear what resolution threshold is most appropriate to distinguish between “good” and “bad” resolution, instead we show maps of temporal resolution with each map of exhumation rate masked below 800 m. Additional data that fall in low-resolution areas and time intervals would improve the resolution of the results. During the earliest time interval, the exhumation rate map is dominated by the prior value of 0.4 km Ma^{-1}. Areas within the western Greater Caucasus that lack cooling age data are predicted to exhume at this rate for the duration of the model and this is an expected artefact of the analysis as reflected by the low resolution values. Towards the present, an increasing number of ages contribute to the exhumation rate output and rates deviate from the prior. As the number of ages constraining rates increases, parts of the western Greater Caucasus decrease in exhumation rate. This does not necessarily mean that there has been a decrease in exhumation rate, rather that in earlier time steps the rates were unconstrained by effective data. In the illustrated model run, well constrained exhumation rates for much of the Miocene are of the order of 0.10-0.15 km Ma^{-1}. Exhumation rate in a specific time interval is constrained by the data that fall within that specific time interval but also exhumation rates in other time intervals. This is because the distance to the closure depth is the integral of the exhumation rate history between the present day and the age of the sample. Therefore, data that fall in earlier time intervals influence all subsequent exhumation rates. Furthermore, if the exhumation rate history of a single age is discretized into two-time intervals, changing the exhumation rate in the younger time interval (due to the inclusion of additional data) forces the exhumation rate in the older time interval to change so that the total exhumation remains constant. This anti-correlation of exhumation rate between time intervals may explain the very low rates in the 9.6-5.33 Ma time interval between Mt. Elbrus and Mt. Kazbek (Figure 10b). This effect is illustrated in Figure 11a-b, where <5.33 Ma cooling ages (that constrain recent rates) were excluded from the model run and the 9.6-5.33 Ma exhumation pattern more closely matches that of earlier time periods.

The main conclusion from the inverse modelling exercise is that whilst phases of modest Oligo-Miocene exhumation are apparent, there was a marked increase in exhumation rate between Mt. Elbrus and Mt. Kazbek during the Pliocene and younger modelled time interval. This increase is consistent with the findings of Avdeev and Niemi [2011]. Exhumation rates also increased farther to the west during this time interval, but by a lesser amount. For instance, in our illustrated model run, well-constrained exhumation rates in the north-eastern sector of the western Greater Caucasus reached ~0.5 km Ma^{-1} or more, whilst in the north-western sector they were closer to 0.25 km Ma^{-1} (Figure 10a). The precise timing of this increase in exhumation rate is conditioned by the time steps chosen for the inverse modelling and is more accurately defined by individual sample thermal models. This study would suggest that increased exhumation rates may have been initiated slightly earlier (at c. 10-8 Ma) in the northwest (Figure 9) than previously modelled in the northeast [at c. 5 Ma; Avdeev and Niemi, 2011]. There is also tentative evidence that a subtle increase in exhumation may have also begun before c. 5 Ma in the latter region, but this has been masked by the later episode of cooling (Figure 11b).

6 Thermal Effects of Regional Magmatism

The region of young FT ages identified by this and earlier studies coincides with that of Middle Miocene to Quaternary magmatism in the Caucasus region (Figure 5d). The oldest magmatism occurred in the Guria [western Adjara-Trialet Belt, c. 15 & 9-7.5 Ma; Lebedev et al., 2009a, 2011b] and Mineral'nyye Vody [Caucasian Mineral Waters, c. 8.3 Ma; Lebedev et al., 2006b] regions to the south and north of the main range, respectively. Magmatism on its southern slope, around the Utsera fault, occurred between c. 7.2-6.0 Ma [Lebedev et al., 2013]. In the core of the western Greater Caucasus it is younger, being concentrated between 4.5-1.6 Ma [Hess et al., 1986; Lebedev et al., 2009b, 2011b, 2006a]. The most recent phase of volcanism in the Mt. Elbrus and Mt. Kazbek regions began around 250 ka ago [Lebedev et al., 2010, 2011a; Lebedev and Vashakidze, 2014]. Magma is generally thought to be mantle derived, as indicated by the Sr-Nd-O isotopic systematics of recent volcanic rocks and the high helium isotopic values of associated subsurface fluids [Polyak et al., 2009, 2000; Tutberidze, 2012]. Polyak et al. [2000] noted a spatial relationship between increasing $^{3}He/^{4}He$ values and background conductive heat flow densities, and decreasing FT ages from the Král and Gurbanov [1996] data set. This relationship remains valid for the more recent thermochronometric and helium isotopic data from the region (Figures 5 & 6) and raises the possibility that the young low temperature thermochronometric cooling ages and mantle-derived Cenozoic magmatism are linked. We shall explore the potential dynamic effects of this mantle-driven magmatism on cooling ages later. Here though we consider whether magma emplacement may have resulted in magmatic heating of the crust, transient changes in regional thermal gradients and an overprinting of the exhumation-induced thermochronometric record.

The thermal effects of shallow-magma emplacement in the western Greater Caucasus are difficult to assess. Volcanic centre locations and ages are catalogued in the supplementary information (Table S1). Pluton sizes are poorly constrained. An exception to this is the shallow magma chamber beneath Mt. Elbrus that has been estimated to be ~9 km in diameter [Milyukov et al., 2010]. Broadly speaking, if heat transfer is mainly by conduction, the zone of heating associated with magma emplacement is localized (extending out ~2-3 times the pluton radius) and will decay back to normal geotherms within 5-10 Myrs depending on pluton size [Murray et al., 2018]. This would suggest that the Elbrus pluton will be associated with a thermal affect extending ~10-15 km from its volcanic centre. The thermal effect of other plutons is likely to be smaller.

There are 15 samples within 10 km of known Neogene to Quaternary magmatic centers (Table S2). These are highlighted on Figures 6 and 8. Of these, it is clear that the AFT and ZFT ages of sample MS_004_3 were reset because of its proximity to the Eldzhurtinskiy granite. The sample is ~6.3 km from the centre of the granite outcrop and ~3.8 km from its closest margin. We have therefore excluded it from the inverse modelling dataset, along with sample 228C of Král and Gurbanov [1996] because of its atypically young (1.0±0.1 Ma) AFT cooling age (Figures 6 & 8). The other highlighted samples do not have systematically younger AFT cooling ages than other samples to the east of Mt. Elbrus; the effects of conductive thermal overprinting from nearby volcanic centres is therefore not obvious.

In addition to possible conductive thermal effects, there is evidence for a widespread convective hydrothermal system associated with magmatism in the central western Greater Caucasus [Polyak et al., 2011]. Masurenkov et al. [2009] studied a network of carbonate-rich mineral water springs around the Elbrus intrusion and identified a large (90-110 km) thermal anomaly associated with it. Spring water temperatures are relatively low (17-22°C) [Masurenkov et al., 2009; Polyak et al., 2009], although these temperatures will have been elevated during initial emplacement [Gazis et al., 1996; Gurbanov et al., 2008].

Resultant heat flow patterns in the western Greater Caucasus are rather poorly constrained. Nevertheless, Polyak et al. [2000] documented a heterogeneous pattern with up to a two-fold increase in heat flow above background around the volcanic centres of Mt. Elbrus and Mt. Kazbek. Increasing the present-day geothermal gradient to 60°C km^{-1} in our inverse model results in the suppression of exhumation rates to a degree that those in the Mt. Elbrus – Mt. Kazbek region are similar to those farther west in our standard model where a present-day geothermal gradient of 38°C km^{-1} was used (cf. the eastern portion of Figure 11c with the western portion of Figure 10a). A scenario with an eastward increase in geothermal gradient by ~50% could, therefore, adequately explain the modelled apparent exhumation pattern in the western Greater Caucasus.

7 Independent Erosion Rate and Uplift Data

In this section, we examine present-day erosional and uplift proxies in the western Greater Caucasus. We do this to test whether they mirror the lateral variations evident in the thermochronometric dataset. Given the uncertainties over the transient thermal effects of magmatism highlighted above, such similarities would help validate the primary geodynamic signal of the thermochronometric data.

7.1 Cosmogenic Isotope Data

Vincent et al. [2011] reported the ^{10}Be cosmogenic nuclide analysis of river sand from the upper reaches of the Inguri River catchment. This indicated average catchment-wide erosion of ~60 cm over the last ~544 yrs. Although there are difficulties in extrapolating cosmogenic erosion rates to geological timescales, this equates to a rate (~1.1±0.3 km Ma^{-1}) similar to that obtained from the AFT analysis of a bedrock sample located farther to the east in the headwaters of the Tskhenis River by Vincent et al. [2011] (~0.9 km Ma^{-1}) (Figure 5c). This independent methodology thus adds weight to the finding that high rates of exhumation have occurred in the south-eastern sector of the western Greater Caucasus in west Georgia since at least the Pleistocene.

7.2 River Sediment Fluxes

Present-day erosion rates for specific catchments in the north-western, south-western and south-eastern sectors of the western Greater Caucasus were calculated by Vezzoli et al. [2014]. They increase south- and east-wards (Table 4; Figure 12). Here, we calculate modern erosion rates for the Baksan catchment, in the north-eastern sector of the range, for which estimates of total river load are also available [Petrakov et al., 2007; Seinova et al., 2011]. The drainage basin is characterized by catastrophic glacial debris flows with high sediment load, triggered by extreme rainfall events (e.g. on 19th July 1983, 83 simultaneous debris flows were formed). The Baksan total average river load is 4.825 ± 2.180 × 10^6 ton a^{-1}. To derive the average erosion rate, this value is divided by the drainage area (6800 km^2) and the density of the material eroded [Ahnert, 1970; Hay, 1998; Hinderer et al., 2013]. A density value of ρ = 2.70 ± 0.03 g cm^{-3} is assumed in our calculations using the same methodology as Vezzoli et al. [2014]. Results indicate that the Baksan catchment has an average erosion rate of 0.26 ±0.12 mm a^{-1}, comparable to that of the Inguri and Rioni rivers to the south (Table 4).

Mean daily runoff decreases from 55.9 l/s·km^2 in the Mzimta basin to 40.6 - 31.6 l/s·km^2 in the Inguri and Rioni catchments respectively, to less than 20 l/s·km^2 in the Baksan catchment [Jaoshvili, 2002; Rets et al., 2018]. In the Kuban Basin it is 7 l/s·km^2 (Mikhailov, 2004). These data run contrary to the general relationship between orographic precipitation and sediment yield and suggest that, regionally, precipitation rate is not the main factor controlling erosion rates. This conclusion was also reached by Vezzoli et al. [2014] and Forte et al. [2016]. Instead, it points to: (1) an eastward increase in rock uplift along the south flank of the range; (2) high rates of rock uplift to the east of Mt. Elbrus in both the north-eastern and south-eastern sectors of the range, and; (3) relatively low rock uplift rates in its north-western sector. This closely mirrors the pattern in model 2 of Vincent *et al*. [2011] (Figure 7) and, within the limits of the thermochronometric coverage, the pattern derived from sector-averaged AFT-derived exhumation rates (Table 4) and this study's inverse thermal modelling (Figure 10a).

7.3 Geomorphic Markers of Uplift

Bedrock rivers are sensitive markers of tectonics and climate through their network geometry, channel slope and discharge [e.g.Castelltort et al., 2012; Kirby and Whipple, 2012; Whipple, 2009]. In particular, the planform and long profile of rivers have long been used to infer tectonic processes in active mountain belts [e.g.Whipple, 2004; Whipple and Meade, 2006; Wobus et al., 2006].

In this study, the geomorphic characteristics of all the main rivers draining the western Greater Caucasus were delineated in *TopoToolbox*, a set of MATLAB functions that support the analysis of relief and flow pathways in digital elevation models [DEM; Schwanghart and Scherler, 2014]. Analysis of the longitudinal profile of bedrock channels, with the calculation of the channel steepness index (k_s; e.g. Whipple, 2004), was carried out on a 30 m-resolution DEM provided by Shuttle Radar Topography Mission Global (SRTM GL1; https://opentopography.org). The channel steepness index, calculated from the power-law relationship $S = k_s A^{-\theta}$ between the local channel slope *S* and the contributing drainage area *A* [a proxy for discharge; Hack, 1957; Flint, 1974], is relatively sensitive to differences in rock uplift rate, climate or substrate lithology and thus represents a useful metric for tectonic geomorphic studies [e.g., Kirby and Whipple, 2001; Wobus et al., 2006]. A fixed reference concavity (θ ref = 0.45) was used to facilitate comparison among channel slopes with widely varying drainage areas and concavities [Snyder et al., 2000; Whipple, 2004; Wobus et al., 2006; Norton and Schlunegger, 2011]. Figure 12 shows the normalized channel steepness index (k_{sn}) for the main rivers of the western Greater Caucasus and the average k_{sn} calculated for the four sectors of the western Greater Caucasus.

Previous studies by Vezzoli et al. [2014] and Forte et al. [2016] on the tectonic geomorphology of the western Greater Caucasus highlighted the close correspondence of the highest k_{sn} values with the highest elevations near the centre of the range (e.g. around Mt. Elbrus). Neither Vezzoli et al. [2014] or Forte et al. [2016] recognized significant lithological or climatic controls on channel steepness. Forte et al. [2016] also highlighted the apparent disconnect between modern climate, shortening rates and topography. They related this to either rock uplift caused by slab detachment or delamination, or to a recent slowing of convergence rates in the western Greater Caucasus.

Rivers draining the northern side of the western Greater Caucasus flow across or obliquely to the main structures / lithological boundaries and yield increasing k_{sn} values towards the east (Figure 12). Specifically, from the Mali Laba to Kuban rivers, k_{sn} varies from 100 to ~150. This increases to ~170 along the Malka and Baksan rivers and to up to ~200 in the upper reaches of the Urukh and Terek rivers (Figure 12). Averaged normalized bedrock channel k_{sn} indices increase from 81±11 in the north-western sector of the range to 140±20 in the north-eastern sector (Figure 12).

Rivers draining the southern side of the range have a complex pattern with a higher proportion of their courses that flow obliquely or subparallel to its structural trend; this is particularly the case in their upper reaches (Figure 12). This is consistent with the higher degree of folding and faulting in Mesozoic strata to the south of the crystalline core of the range that, in turn, is a result of the inversion of the Greater Caucasus Basin and the predominantly south-vergent nature of the range (Figure 3). Average normalized bedrock channel k_{sn} indices are homogeneously high in south-western (120±40) and south-eastern (137±21) sectors of the range and are similar to that in the north-eastern sector (Figure 12). Maximum K_{sn} values were calculated in the Inguri River upstream of its dam site (~230) where its catchment-wide erosion rate, derived from cosmogenically data, is equivalent to ~1.1 mm a^{-1} [Vincent et al., 2011].

The spatial variation in K_{sn} values broadly mirrors the thermochronometric and sediment flux data (Table 4). This would suggest that any shallow-level magmatically-induced thermal perturbations have not reset the overall thermochronometric pattern in the western Greater Caucasus and that this instead reflects variations in exhumation.

8 Discussion

In this section, we examine possible controls for the spatial and temporal variations in western Greater Caucasus exhumation identified in this study. We then go on to briefly interpret the cooling history of the eastern Greater Caucasus in the light of these insights.

8.1 Controls on Spatial Variations in Exhumation in the Western Greater Caucasus

8.1.1. Differential Cooling due to Variations in Crustal Shortening

Although poorly constrained by FT data, geologic and geomorphic evidence indicate a relatively continuous zone of tectonic shortening, uplift and exhumation along the southern slope of the western Greater Caucasus. This is exemplified by the Racha earthquake, by geomorphic studies at the outermost thrust front in the Rioni Basin [Tibaldi et al., 2017a, 2017b] (Figure 2) and by the presence of growth anticlines with antecedent drainage and wind gaps north of Suchumi (Figure 13). This is within what has previously been modelled as stable Eurasia (Figure 4).

The region of high exhumation identified in this and earlier thermochronometric studies occurs to the north of this, in the crystalline core of the range between Mt. Elbrus and Mt. Kazbek. Immediately to the west of Mt. Elbrus, AFT data display a marked increase in cooling age (Figures 5a-b & 6). This indicates an abrupt westward decrease in exhumation rate (Figure 10a) and confirms exhumation model 2 of Vincent et al. [2011] (Figure 7). A kinematic explanation for this decrease in exhumation rate is not obvious for two reasons. Firstly, along strike GPS-derived velocity data are not currently of sufficient resolution to be able to determine whether there is a change in the present day velocity field in the vicinity of Mt. Elbrus (Figure 1). This makes it difficult to attribute the marked change in AFT cooling ages, modelled exhumation rates and k_{sn} values observed at this position to differences in surface velocities unless they have recently changed. Similarly, serial balanced cross sections across the range have yet to be constructed to constrain whether there is a marked variation in overall shortening at this position. Secondly, even if variations in crustal shortening were better constrained, it is unclear how this could be partitioned, north of a zone of likely uniform shortening, within the core of the western Greater Caucasus to generate the observed lateral variations in exhumation. Given these uncertainties, alternative controls for the differential exhumation of the crystalline core of the western Greater Caucasus need to be considered.

8.1.2 Differential Cooling due to Variations in Thermally Induced Rock Uplift

The region of younger AFT cooling ages in the core of the western Greater Caucasus broadly corresponds with that of Pliocene and younger magmatism. Helium isotope data suggest that this magmatism is mantle derived [Polyak et al., 2000] (Figures 5d & 6).

Tomographic models typically characterize the Caucasus and Eastern Anatolia as a region containing a low velocity crust and uppermost mantle lid between the higher velocity regions of Arabia to the south and the East European Craton to the north [Al-Lazki et al., 2004; Koulakov et al., 2012; Mutlu and Karabulut, 2011; van der Meer et al., 2018]. In the Caucasus, this low velocity zone is generally attributed to asthenospheric replacement of mantle lithosphere following either delamination or slab break-off [Koulakov et al., 2012; van der Meer et al., 2018; Zabelina et al., 2016; Zor, 2008]. The resolution of these tomographic models is typically low, although the studies of Zor [2008], Mutlu and Karabulut [2011], and Koulakov et al. [2012] all highlighted the presence of low velocity anomalies in the uppermost mantle roughly coincident with the volcanic centres at Mt. Elbrus and Mt. Kazbek. The microseismic studies of Gorbatikov et al. [2015] and Rogozhin et al. [2016] and the tomographic study of Zabelina et al. [2016] also identified low velocity zones in the crust beneath the Elbrus and Kazbek volcanic centres.

Asthenospheric upwelling and magma intrusion is a plausible explanation for the increased rock uplift and exhumation in the core of the range. This is our preferred control given the lack of an obvious geodynamic driver; however, a number of issues remain.

Firstly, the lateral extent of magmatism is much more limited than the region of proposed slab detachment [Mumladze et al., 2015; van der Meer et al., 2018] or delamination [Ershov et al., 1999]. One possible explanation for the limited lateral distribution, but north-south extension of magmatism is small-scale toroidal flow around the western edge of the eastern Greater Caucasus down-going slab, located to the east of Mt. Kazbeg, following western slab break-off [Mumladze et al., 2015].

Secondly, the rapid decrease in exhumation rates west of Mt. Elbrus does not fit with typical models of asthenospheric upwelling that affect large areas, having wavelengths of hundreds of kilometers. Despite this, much shorter wavelength variations in exhumation by the dynamic support of the lithosphere are possible in areas of highly heterogeneous crust [Cloetingh et al., 2013]. Král and Gubanov [1996] related the abrupt change in AFT ages that they observed to activity on an Elbrus fault system. There is no surface or seismic expression of this fault system (Figures 1 & 2) and additional evidence is needed. Nevertheless, an aseismic transverse basement trend passing through Mt. Elbrus could be the cause of a localized density-induced exhumation gradient at the western margin of the Elbrus-Kazbek magmatic zone. If present, this basement trend may form a continuation of the eastern boundary of the Stavropol High. There is a marked change in crustal affinity across this boundary with an eastward decrease, into the Terek-Caspian depression, in crystalline crustal thickness that Kostyuchenko et al. [2004] attributed to a Paleozoic transform fault (Figure 1).

Lastly, whilst there is undoubtedly a complex thermal heterogeneity to the crust and upper mantle of the western Greater Caucasus, specific spatial patterns cannot be matched precisely to the thermochronometric data. For instance, Zabelina et al. [2016] highlighted a region of low velocity crust beneath Mt. Elbrus that extends at least 100 km to its west-northwest into the region typified by older AFT cooling ages. Further work is clearly required.

In is unclear how asthenospheric upwelling, the postulated cause of increased Pliocene uplift and exhumation in the north-eastern sector of the western Greater Caucasus, will have affected the region farther south. A young AFT and old ZFT age from metasediments to the north of the Racha-Lechkumi fault in the south-eastern sector of the range would suggest that rapid exhumation of the fill of the Greater Caucasus Basin has probably been on-going since the Pliocene [Vincent et al., 2011] (Figure 8b). However, shortening along the southern slope of the western Greater Caucasus began in the Eocene, such that either shortening rates must have increased dramatically in the recent past or exhumation in this region resulted from a combination of both longer-term tectonic shortening and more recent crustal buoyancy. Similar or slightly older AFT cooling ages within the crystalline core of the north-eastern sector of the western Greater Caucasus indicate that there has not been significant differential rock uplift across the Main Caucasus Thrust, which divides these two regions, during the Pliocene [cf. Avdeev and Niemi, 2011] (Figure 8b). This could be attributed to the effects of asthenospheric upwelling on both regions. One test of this hypothesis would be if AFT cooling ages within the south-western sector of the western Greater Caucasus turn out to be systematically older than those farther east; these data are not currently available.

8.2 Controls on Temporal Variations in Exhumation in the Western Greater Caucasus

This work supports earlier thermochronometric studies in identifying low to moderate rates of punctuated Oligo-Miocene exhumation in the western Greater Caucasus. It also confirms the Pliocene increase in exhumation reported by Avdeev and Niemi [2011] between Mt. Elbrus and Mt. Kazbek, and identifies a lower magnitude increase in exhumation farther west that may have begun earlier, in the Late Miocene.

The timing of cooling events in the western Greater Caucasus do not imply causation and, therefore, the findings of this study cannot be used as definitive support for either an Eocene-Oligocene transition or Pliocene age for Greater Caucasus Basin closure. Consequently, Oligo-Miocene cooling in the crystalline core of the range could reflect uplift and exhumation of the (former) northern flank of the western Greater Caucasus Basin following its closure [Vincent et al., 2016, 2011] or, conceivably, active subduction of a much wider oceanic basin beneath this margin [Cowgill et al., 2016]. Insight into which scenario is more likely will rely on the integration of multiple lines of complementary evidence.

Evidence in support of both models have been presented elsewhere [Cowgill et al., 2018, 2016; Vincent et al., 2016, 2018] and is not repeated here.

The Late Miocene and / or Pliocene increase in cooling in the western Greater Caucasus is broadly coincident with a widespread reorganization of the Arabia-Eurasia collision zone. This was first noted by Axen et al. [2001] and Allen et al. [2004] and estimated to begin at c. 5±2 Ma. Subsequent studies are beginning to establish a longer, c. 12-4 Ma, interval of reorganization and/or increased exhumation, largely from observations in the Zagros [e.g. Barber et al., 2018; Gavillot et al., 2010; Mouthereau, 2011], Alborz [e.g. Guest et al., 2006; Rezaeian et al., 2012] and Talesh [Madanipour et al., 2017]. The precise cause of this reorganization is unclear. Models include final Arabia-Eurasia suturing [i.e. ‘hard collision’; Axen et al., 2001; Barber et al., 2018], which could include Greater Caucasus Basin closure, a switch from a free to constrained eastern margin of the collision zone [Allen et al., 2011], Neotethyan slab-break off [Agard et al., 2011; Keskin, 2003] or the initiation of Anatolian extrusion [Westaway, 1994]. Given the size and complexity of the region and the diachronous nature of events, it is likely that a number of potentially interlinked processes will have been responsible.

With regard to the increased Late Miocene to Pliocene cooling rates observed in the core of the western Greater Caucasus, asthenospheric upwelling, potentially due to slab break off [Mumladze et al., 2015; van der Meer et al., 2018], is our preferred explanation. This could generate the observed magmatism and additional dynamic uplift, and thus exhumation above regional compressional-related rates, although as pointed out earlier this would require crustal heterogeneities to modulate the wavelength of these processes. A 20-25 Ma delay between continental collision and slab break off [van Hunen and Allen, 2011], would make this process compatible with Greater Caucasus Basin closure around the Eocene-Oligocene transition.

8.3 Implications of Thermochronometric Data from the Eastern Greater Caucasus

Two PhD studies on the eastern Greater Caucasus of central Azerbaijan incorporated thermochronometric analyses [Avdeev, 2011; Bochud, 2017] (Figure 1). These provide additional insights into the timing of exhumation in the range as a whole.

Avdeev [2011] performed three AFT analyses with resultant central ages ranging between 88-14 Ma. Seven of his eight AHe analyses yielded much younger average ages (4.0-1.7 Ma), although it is not possible to determine the validity of the grain averaging process because of a lack of reported dispersion and grain size data. The thermal histories of three samples were modelled, two from Early to Middle Jurassic sediments from the northern flank of the eastern Greater Caucasus and one from Paleocene-Eocene volcaniclastic sediments from its southern flank. They all show an increase in cooling around 6-5 Ma.

Bochud [2017] carried out seven AFT analyses on Aalenian sandstones from the central and northern parts of the eastern Greater Caucasus. Central ages ranged between 90-13 Ma. Four samples contained sufficient track lengths for modelling and indicate that initial exhumation began around 28-20 Ma (~0.12 km Ma^{-1}) and accelerated between 9-5 Ma (~0.38-0.53 km Ma^{-1}), peaking in one instance at ~1.91 km Ma^{-1} between 3-2 Ma.

These cooling histories share some similarities to those farther west within the core of the western Greater Caucasus, although it should be borne in mind that these studies are rather distant from (>375 km), and in different present-day geodynamic regimes (Figure 1) to, each other. Caution should therefore be exercised to avoid over emphasis of the significance of these data. Nevertheless, it is plausible that the acceleration in cooling rates documented in the eastern Greater Caucasus is a response to wider Arabia-Eurasia reorganization and, when data become available, will mirror cooling histories from the southern slope of the western Greater Caucasus. Subtle evidence for this increase in cooling is also present in the north-western sector of the western Greater Caucasus (at c. 10-8 Ma), but have been overprinted in the north-eastern sector by the slightly younger (c. 5 Ma) buoyancy effects of mantle upwelling.

9 Conclusions

The thermochronometric analysis of 21 samples from the crystalline core of the western Greater Caucasus supports earlier work in highlighting a marked lateral change in Cenozoic cooling rates around the position of Mt. Elbrus, the westernmost volcanic centre in the range. The average AFT age of the crystalline basement of the range to the west of Mt. Elbrus is 32.5 Ma, whilst to the east it is 6.3 Ma. Assuming an average geothermal gradient of 40°C km^{-1}, AFT cooling ages as young as 2.4 Ma indicate that exhumation rates in excess of 1 km Ma^{-1} occurred locally to the east of Mt. Elbrus. ZFT analysis record Mesozoic and Late Palaeozoic cooling ages from the same region that, with the same geothermal gradient, necessitates less than 5 km of overall exhumation and implies that the current rates of exhumation cannot have begun more than c. 5-7 Myrs ago. This is reflected in the inverse modelling of the compiled thermochronometric data that highlights a region of rapid exhumation between Mt. Elbrus and Mt. Kazbek during the Pliocene. An increase in exhumation also occurred to the west of this region, but at approximately less than half the rate. Thermal modelling of individual samples in the western Greater Caucasus suggest that this increase in cooling rate may have initiated slightly earlier in the west of the region (at c.

10-8 Ma) than in the east (at c. 5 Ma). GPS-derived velocity records of the southern slope of the western Greater Caucasus indicate that shortening rates do not vary on either side Mt. Elbrus, casting doubt on whether tectonic shortening, uplift and exhumation are the drivers of the observed variations in cooling rates.

The region with young low temperature thermochronometric cooling ages between Mt. Elbrus and Mt. Kazbek coincides with that of active Caucasian mantle-sourced Late Miocene and younger magmatism. However, normalized channel-steepness indices, sediment flux and depositional rate evidence mirror the AFT data and indicate that the fission track ages reflect exhumation-driven cooling rather than simply thermal relaxation or overprinting.

Magmatism in the western Greater Caucasus may have been triggered by the asthenospheric replacement of lithospheric mantle due to upwelling. The buoyancy effects of this low-density material is capable of causing the magnitude of exhumation and cooling recorded in the fission track data.

Uplift patterns generated by thermally-induced dynamic uplift typically occur over wavelengths of several 100 km, suggesting that if this is the case here, important basement structures must have been active to effectively partition this uplift over shorter wavelengths. These heterogeneities may be related to the same structures responsible for the Stavropol High to the north of the Caucasus. However, further research is required. Given the heterogeneous nature of most continental lithosphere, our model of mantle-supported uplift with differential exhumation controlled by crustal structure may well be applicable to other mountain belts worldwide.

References

Adamia, S. A., Akhvlediani, K. T., Kilasonia, V. M., Nairn, A. E. M., Papava, D., & Patton, D. K. (1992), Geology of the Republic of Georgia: a review, *International Geology Review*, *34*(5), 447-476, https://doi.org/10.1080/00206819209465614.

Adamia, S. A., Alania, V., Chabukiani, A., Kutelia, Z., & Sadradze, N. (2011), Great Caucasus (Cavcasioni): a long-lived north-Tethyan back-arc basin, *Turkish Journal of Earth Sciences*, *20*, 611-628, https://doi.org/10.3906/yer-1005-12.

Agard, P., Omrani, J., Jolivet, L., Whitechurch, H., Vrielynck, B., Spakman, W., Monié, P., Meyer, B., & Wortel, R. (2011), Zagros orogeny: a subduction-dominated process, *Geological Magazine*, *148*(5-6), 692-725, https://doi.org/10.1017/s001675681100046x.

Ahnert, F. (1970), Functional relationships between denudation, relief and uplift in large mid-latitude drainage basins, *American Journal of Science*, *268*, 243–263.

Al-Lazki, A. I., Sandvol, E., Seber, D., Barazangi, M., Turkelli, N., & Mohamad, R. (2004), *Pn* tomographic imaging of mantle lid velocity and anisotropy at the junction of the Arabian, Eurasian and African plates, *Geophysical Journal International*, *158*, 1024-1040.

Allen, M. B., Jackson, J. A., and Walker, R. (2004), Late Cenozoic reorganization of the Arabia-Eurasia collision and the comparison of short-term and long-term deformation rates, *Tectonics*, *23*(2), TC2008, https://doi.org/10.1029/2003TC001530.

Allen, M. B., Jones, S., Ismail-Zadeh, A., Simmons, M., & Anderson, L. (2002), Onset of subduction as the cause of rapid Pliocene-Quaternary subsidence in the South Caspian basin, *Geology*, *30*(9), 775-778, https://doi.org/10.1130/0091-7613(2002)030<0775:oosatc>2.0.co;2.

Allen, M. B., Kheirkhah, M., Emami, M. H., & Jones, S. J. (2011). Right-lateral shear across Iran and kinematic change in the Arabia-Eurasia collision zone, *Geophysical Journal International*, *184*(2), 555-574, https://doi.org/10.1111/j.1365-246X.2010.04874.x.

Allen, M. B., Vincent, S. J., Alsop, G. I., Ismail-Zadeh, A., & Flecker, R. (2003), Late Cenozoic deformation in the South Caspian region: effects of a rigid basement block within a collision zone, *Tectonophysics*, *366*, 223-239.

Avdeev, B. (2011), Tectonics of the Greater Caucasus and the Arabia-Eurasia orogen, University of Michigan.

Avdeev, B., & Niemi, N. A. (2011), Rapid Pliocene exhumation of the central Greater Caucasus constrained by low-temperature thermochronometry, *Tectonics*, *30*(2), TC2009, https://doi.org/10.1029/2010TC002808.

Axen, G. J., Lam, P. S., Grove, M., Stockli, D. F., & Hassanzadeh, J. (2001), Exhumation of the west-central Alborz Mountains, Iran, Caspian subsidence, and collision-related tectonics, *Geology*, *29*(6), 559-562, https://doi.org/10.1130/0091-7613(2001)029<0559:eotwca>2.0.co;2.

Ballato, P., Landgraf, A., Schildgen, T. F., Stockli, D. F., Fox, M., Ghassemi, M. R., Kirby, E., & Strecker, M. R. (2015), The growth of a mountain belt forced by base-level fall: Tectonics and surface processes during the evolution of the Alborz Mountains, N Iran, *Earth and Planetary Science Letters*, *425*(0), 204-218, http://dx.doi.org/10.1016/j.epsl.2015.05.051.

Banks, C. J., Robinson, A. G., & Williams, M. P. (1997), Structure and regional tectonics of the Achara-Trialet Fold Belt and the adjacent Rioni and Kartli foreland basins, Republic of Georgia, In A. G. Robinson (Ed.), *Regional and Petroleum Geology of the Black Sea and*

Surrounding Region, (Vol. 68*,* pp. 331-346). Tulsa, Oklahoma, AAPG Memoir, https://doi.org/10.1306/M68612C17.

Barber, D. E., Stockli, D. F., Horton, B. K., & Koshnaw, R. I. (2018), Cenozoic Exhumation and Foreland Basin Evolution of the Zagros Orogen During the Arabia-Eurasia Collision, Western Iran, *Tectonics*, *37*(12), 4396-4420, https://doi.org/10.1029/2018TC005328.

Baskakova, G. V., & Nikishin, A. M. (2018), The geological history of the Kerch-Taman area based on a reconstructed regional balanced section, *Moscow University Geology Bulletin*, *73*(5), 416-422.

Bochud, M. (2017), Tectonics of the Eastern Greater Caucasus in Azerbaijan, PhD thesis, 197 pp, University of Fribourg (Switzerland).

Brunet, M.-F., Korotaev, M. V., Ershov, A. V., & Nikishin, A. M. (2003), The South Caspian Basin: a review of its evolution from subsidence modelling, *Sedimentary Geology*, *156*, 119-148, https://doi.org/10.1016/S0037-0738(02)00285-3.

Castelltort, S., Goren, L., Willett, S. D., Champagnac, J.-D., Herman, F., & Braun, J. (2012), River drainage patterns in the New Zealand Alps primarily controlled by plate tectonic strain, *Nature Geoscience*, *5*(10), 744-748.

Chernyshev, I. V., Bubnov, S. N., Lebedev, V. A., Gol'tsman, Y. V., Bairova, E. D., & Yakushev, A. I. (2014), Two stages of explosive volcanism of the Elbrus area: Geochronology, petrochemical and isotopic-geochemical characteristics of volcanic rocks, and their role in the neogene-quaternary evolution of the Greater Caucasus, *Stratigraphy and Geological Correlation*, *22*(1), 96-121, https://doi.org/10.1134/s086959381401002x.

Cloetingh, S., Burov, E., & Francois, T. (2013), Thermo-mechanical controls on intra-plate deformation and the role of plume-folding interactions in continental topography, *Gondwana Research*, *24*(3), 815-837, https://doi.org/10.1016/j.gr.2012.11.012.

Copley, A., & Jackson, J. (2006), Active tectonics of the Turkish-Iranian Plateau, *Tectonics*, *25*, https://doi.org/10.1029/2005TC001906.

Cowgill, E., Forte, A. M., Niemi, N., Avdeev, B., Tye, A., Trexler, C., Javakhishvili, Z., Elashvili, M., & Godoladze, T. (2016), Relict basin closure and crustal shortening budgets during continental collision: An example from Caucasus sediment provenance, *Tectonics*, *35*, 2918-2947, https://doi.org/10.1002/2016TC004295.

Cowgill, E., Niemi, N. A., Forte, A. M., & Trexler, C. C. (2018), Reply to Comment by Vincent et al, *Tectonics*, *37*(3), 1017-1028, https://doi.org/10.1002/2017tc004793.

Dotduyev, S. I. (1986), The nappe structure of the Greater Caucasus, *Geotectonics*, *20*, 420-430.

Dzhanelidze, A. I., & Kandelaki, N. A. (1955), Geological map of the USSR, Caucasus series sheet K-38-XIII (scale 1:200,000). Moscow, Ministry of Geology.

Ehlers, T. A., Chaudhri, T., Kumar, S., Fuller, C. W., Willet, S. D., Ketcham, R. A. et al. (2005), Computational tools for low-temperature thermochronometric interpretation, In P. W. Reiners & T. A. Ehlers (Eds.), *Low-Temperature Thermochronology: Techniques, Interpretations, and Applications*, (Vol. 58, pp. 589-622). Chantilly, VA, Reviews in Mineralogy and Geochemistry.

Engdahl, E. R., & Villaseñor, A. (2002), Global Seismicity: 1900-1999, In W. H. K. Lee, H. Kanamori, P. C. Jennings & C. Kisslinger (Eds.), *International Handbook of Earthquake and Engineering Seismology*, (Part A, Chapter 41, pp. 665-690), Academic Press.

Ershov, A. V., Brunet, M. F., Korotaev, M. V., Nikishin, A. M., & Bolotov, S. N. (1999), Late Cenozoic burial history and dynamics of the Northern Caucasus molasse basin: implications for foreland basin modelling, *Tectonophysics*, *313*(1-2), 219-241.

Flint, J. J. (1974), Stream gradient as a function of order, magnitude, and discharge, *Water Resources Research*, *10*, 969–973.

Forte, A. M., Cowgill, E., Bernardin, T., Kreylos, O., & Hamann, B. (2010), Late Cenozoic deformation of the Kura fold-thrust belt, southern Greater Caucasus, *Geological Society of America Bulletin*, *122*(3-4), 465-486, https://doi.org/10.1130/b26464.1.

Forte, A. M., Cowgill, E., & Whipple, K. X. (2014), Transition from a singly- to doubly-vergent wedge in a young orogen: The Greater Caucasus, *Tectonics*, *33*(11), 2077-2101, https://doi.org/10.1002/2014tc003651.

Forte, A. M., Whipple, K. X., Bookhagen, B., & Rossi, M. W. (2016), Decoupling of modern shortening rates, climate, and topography in the Caucasus, *Earth and Planetary Science Letters*, *449*, 282-294, http://dx.doi.org/10.1016/j.epsl.2016.06.013.

Fox, M., Herman, F., Willett, S. D., & May, D. A. (2014), A linear inversion method to infer exhumation rates in space and time from thermochronometric data, *Earth Surface Dynamics*, *2*, 47-65.

Fox, M., Herman, F., Willett, S. D., & Schmid, S. M. (2016), The exhumation history of the European Alps inferred from linear inversion of thermochronometric data, *American Journal of Science*, *316*(6), 505-541, https://doi.org/10.2475/06.2016.01.

Fuenzalida, H., Rivera, L., Haessler, H., Legrand, D., Philip, H., Dorbath, L., McCormack, D., Arefiev, S., Langer, C., & Cisternas, A. (1997), Seismic source study of the Racha-Dzhava (Georgia) earthquake from aftershocks and broad-band teleseismic body-wave records: an example of active nappe tectonics, *Geophysical Journal International*, *130*(1), 29-46, https://doi.org/10.1111/j.1365-246X.1997.tb00985.x.

Galbraith, R. F., & Laslett, G. M. (1993), Statistical models for mixed fission track ages, *Nuclear Tracks and Radiation Measurement*, *21*, 459-470.

Gallagher, K. (2012), Transdimensional inverse thermal history modelling for quantitative thermochronology, *Journal of Geophysical Research*, *117*, B02408, https://doi.org/doi:10.1029/2011JB00882.

Gavillot, Y., Axen, G. J., Stockli, D. F., Horton, B. K., & Fakhari, M. D. (2010), Timing of thrust activity in the High Zagros fold-thrust belt, Iran, from (U-Th)/He thermochronometry, *Tectonics*, *29*, 25, https://doi.org/10.1029/2009tc002484.

Gazis, C. A., Lanphere, M., Taylor, H. P., & Gurbanov, A. (1995), $^{40}Ar/^{39}Ar$ and $^{18}O/^{16}O$ studies of the Chegem ash-flow caldera and the Eldjurta Granite: cooling of two late Pliocene igneous bodies in the Greater Caucasus Mountains, Russia, *Earth and Planetary Science Letters*, *134*(3-4), 377-391.

Gazis, C., Taylor, H. P., Hon, K., & Tsvetkov, A. (1996), Oxygen isotopic and geochemical evidence for a short-lived, high-temperature hydrothermal event in the Chegem caldera, Caucasus mountains, Russia, *Journal of Volcanology and Geothermal Research*, *73*(3-4), 213-244.

Gorbatikov, A. V., Rogozhin, E. A., Stepanova, M. Yu., Kharazova, Yu V., Andreeva, N. V., Perederin, F. V. et al. (2015), The pattern of deep structure and recent tectonics of the Greater Caucasus in the Ossetian sector from the complex geophysical data, *Izvestiya, Physics of the Solid Earth*, *51*(1), 26-37, https://doi.org/10.1134/s1069351315010073.

Gradstein, F. M., Ogg, J. G., Schmitz, M. D., & Ogg, G. M. (Eds.) (2012), *A Geologic Time Scale* 2012, 1144 pp.). Oxford, Elsevier.

Guest, B., Stockli, D. F., Grove, M., Axen, G. J., Lam, P. S., & Hassanzadeh, J. (2006), Thermal histories from the central Alborz Mountains, northern Iran: Implications for the spatial and temporal distribution of deformation in northern Iran, *Geological Society of America Bulletin*, *118*(11-12), 1507-1521, https://doi.org/10.1130/b25819.1.

Gurbanov, A. G., Bogatikov, O. A., Dokuchaev, A. Y., Gazeev, V. M., Abramov, S. S., Groznova, E. O., & Shevchenko, A. V. (2008), Ore-bearing hydrothermal metasomatic processes in the Elbrus volcanic center, the northern Caucasus, Russia, *Geol. Ore Deposits*, *50*(3), 199-217, https://doi.org/10.1134/s1075701508030033.

Hack, J. T. (1957), Studies of longitudinal stream profiles in Virginia and Maryland. US Geological Survey Professional Paper 294-B, 45–97. Reston (VA), US Geological Survey.

Harkins, N., Kirby, E., Heimsath, A., Robinson, R., & Reiser, U. (2007), Transient fluvial incision in the headwaters of the Yellow River, northeastern Tibet, China, *Journal of Geophysical Research: Earth Surface (2003–2012)*, *112*(F3).

Hay, W. W. (1998), Detrital sediment fluxes from continents to oceans, *Chemical Geology*, *145*, 287–323.

Hess, J. C., Lippolt, H. J., & Borsuk, A. M. (1986), The Neogene volcanism of the Northern Great Caucasus. Isotope and age studies on rift-related alkali rhyolites, *Neues Jahrbuch Fur Mineralogie-Monatshefte*, *156*(1), 63-80.

Hess, J. C., Lippolt, H. J., Gurbanov, A. G., & Michalski, I. (1993), The cooling history of the late Pliocene Eldzhurtinskiy granite (Caucasus, Russia) and the thermochronological potential of grain-size / age relationships, *Earth and Planetary Science Letters*, *117*(3-4), 393-406.

Hinderer, M., Kastowski, M., Kamelger, A., Bartolini, C., & Schlunegger, F. (2013), River loads and modern denudation of the Alps - A review, *Earth-Science Reviews*, *118*, 11–44, https://doi.org/10.1016/j.earscirev.2013.01.001.

Hurford, A. J. (1990), Standardization of fission track dating calibration: recommendation by the Fission Track Working Group of the IUGS subcommission on geochronology, *Chemical Geology*, *80*, 177-178.

Jackson, J. (1992), Partitioning of strike-slip and convergent motion between Eurasia and Arabia in Eastern Turkey and the Caucasus, *Journal of Geophysical Research*, *97*(B9), 12471-12479, https://doi.org/10.1029/92JB00944.

Jackson, J., Priestley, K., Allen, M., & Berberian, M. (2002), Active tectonics of the South Caspian Basin, *Geophysics Journal International*, *148*, 214-245.

Jaoshvili, S. (2002), The Rivers of the Black Sea, *Technical Report Rep. 71*, 58 pp, Copenhagen, European Environment Agency.

Jones, R. W., & Simmons, M. D. (1997), A review of the stratigraphy of Eastern Paratethys (Oligocene-Holocene), with particular emphasis on the Black Sea, In A. G. Robinson (Ed.), *Regional and Petroleum Geology of the Black Sea and Surrounding Region*, (Vol. 68, pp. 39-52). Tulsa, Oklahoma, AAPG Memoir, https://doi.org/10.1306/M68612C4.

Karakhanyan, A., Vernant, P., Doerflinger, E., Avagyan, A., Philip, H., Aslanyan, R. et al. (2013), GPS constraints on continental deformation in the Armenian region and Lesser Caucasus, *Tectonophysics*, *592*(0), 39-45, http://dx.doi.org/10.1016/j.tecto.2013.02.002.

Kazmin, V. G., Sbortshikov, I. M., Ricou, L.-E., Zonenshain, L. P., Boulin, J., & Knipper, A. L. (1986), Volcanic belts as markers of the Mesozoic-Cenozoic active margin of Eurasia, *Tectonophysics*, *123*, 123-152, https://doi.org/10.1016/0040-1951(86)90195-2.

Keskin, M. (2003), Magma generation by slab steepening and breakoff beneath a subduction-accretion complex: An alternative model for collision-related volcanism in Eastern Anatolia, Turkey, *Geophys. Res. Lett.*, *30*(24), 8046, https://doi.org/10.1029/2003gl018019.

Kirby, E., & Whipple, K. (2001), Quantifying differential rock-uplift rates via stream profile analysis, *Geology*, *29*(5), 415-418, https://doi.org/10.1130/0091-7613(2001)029<0415:QDRURV>2.0.CO;2.

Kirby, E., & Whipple, K. X. (2012), Expression of active tectonics in erosional landscapes, *Journal of Structural Geology*, *44*(0), 54-75, http://dx.doi.org/10.1016/j.jsg.2012.07.009.

Kostyuchenko, S. L., Morozov, A. F., Stephenson, R. A., Solodilov, L. N., Vedrentsev, A. G., Popolitov, K. E., Aleshina, A. F., Vishnevskaya, V. S., & Yegorova, T. P. (2004), The evolution of the southern margin of the East European Craton based on seismic and potential field data, *Tectonophysics*, *381*(1-4), 101-118.

Koulakov, I., Zabelina, I., Amanatashvili, I., & Meskhia, V. (2012), Nature of orogenesis and volcanism in the Caucasus region based on results of regional tomography, *Solid Earth*, *3*(2), 327-337, https://doi.org/10.5194/se-3-327-2012.

Král, J., & Gurbanov, A. G. (1996), Apatite fission track data from the Great Caucasus pre-Alpine basement, *Chemie Der Erde-Geochemistry*, *56*(2), 177-192.

Lebedev, V. A., Bubnov, S. N., Chernyshev, I. V., Gol'tsman, Y. V., Chugaev, A. V., & Vashakidze, G. T. (2006a), Pliocene granitoid massif in the Kazbek volcanic center: first geochronological and isotope-geochemical data, *Doklady Earth Sciences*, *411*(2), 1393-1397.

Lebedev, V., Bubnov, S., Chernyshev, I., Chugaev, A., Goltzman, Y., Vashakidze, G., & Bairova, E. (2009b), Geochronology and genesis of the young (Pliocene) granitoids of the Greater Caucasus: Dzhimara multiphase Massif of the Kazbek neovolcanic area, *Geochemistry International*, *47*(6), 550-567, https://doi.org/10.1134/s0016702909060020.

Lebedev, V. A., Chernyshev, I. V., Avdeenko, A. S., Nosova, A. A., Dokuchaev, A. Y., Oleinikova, T. I., & Gol'tsman, Y. V. (2006b), Heterogeneity of Ar and Sr initial isotopic composition in the coexisting minerals from Miocene hypabyssal granitoids in the Caucasian Mineral Waters region, *Doklady Earth Sciences*, *410*(1), 1070-1074, https://doi.org/10.1134/s1028334x06070154.

Lebedev, V. A., Chernyshev, I. V., Dudauri, O. Z., Vashakidze, G. T., Goltsman, Y. V., Bairova, E. D., & Yakushev, A. I. (2013), Manifestations of Miocene acid intrusive magmatism on the southern slope of the Greater Caucasus: First evidence from isotope geochronology, *Doklady Earth Sciences*, *450*(1), 550-555, https://doi.org/10.1134/s1028334x13050103.

Lebedev, V. A., Chernyshev, I. V., & Sharkov, E. V. (2011b), Geochronological scale and evolution of late Cenozoic magmatism within the Caucasian segment of the alpine belt, *Doklady Earth Sciences*, *441*(2), 1656-1660, https://doi.org/10.1134/s1028334x11120051.

Lebedev, V., Sakhno, V., & Yakushev, A. (2009a), Late Cenozoic volcanic activity in western Georgia: Evidence from new isotope geochronological data, *Doklady Earth Sciences*, *427*(1), 819-825, https://doi.org/10.1134/s1028334x09050249.

Lebedev, V., Sakhno, V., & Yakushev, A. (2010), Total duration and spatial migration of Quaternary volcanism in the El'brus region, Greater Caucasus, *Doklady Earth Sciences*, *430*(1), 80-85, https://doi.org/10.1134/s1028334x10010186.

Lebedev, V. A., & Vashakidze, G. T. (2014), The catalogue of Quaternary volcanoes of the Greater Caucasus based on geochronological, volcanological and isotope-geochemical data, *J. Volcanolog. Seismol.*, *8*(2), 93-107, https://doi.org/10.1134/s0742046314020043.

Lebedev, V., Vashakidze, G., Arutyunyan, E., & Yakushev, A. (2011a), Geochronology and evolution of Quaternary volcanism at the Keli Highland, Greater Caucasus, *Geochemistry International*, *49*(11), 1120-1144, https://doi.org/10.1134/s0016702911090035.

Madanipour, S., Ehlers, T. A., Yassaghi, A., & Enkelmann, E. (2017), Accelerated middle Miocene exhumation of the Talesh Mountains constrained by U-Th/He thermochronometry: Evidence for the Arabia-Eurasia collision in the NW Iranian Plateau, *Tectonics*, *36*(8), 1538-1561, https://doi.org/10.1002/2016tc004291.

Masurenkov, Y., Sobisevich, A., Likhodeev, D., & Shevchenko, A. (2009), Thermal anomalies of the Northern Caucasus, *Doklady Earth Sciences*, *429*(1), 1318-1321, https://doi.org/10.1134/s1028334x09080170.

Mellors, R. J., Jackson, J., Myers, S., Gok, R., Priestley, K., Yetirmishli, G., Turkelli, N., & Godoladze, T. (2012), Deep earthquakes beneath the Northern Caucasus: evidence of active or recent subduction in Western Asia, *Bulletin of the Seismological Society of America*, *102*(2), 862-866, https://doi.org/10.1785/0120110184.

Melnikov, V. A., & Popova, E. J. (1966), Geological map of the USSR, Caucasus series sheet K-38-VIII (scale 1:200,000). Moscow, Ministry of Geology.

Mikhailov, V. O., Panina, L. V., Polino, R., Koronovsky, N. V., Kiseleva, E. A., Klavdieva, N. V., & Smolyaninova, E. I. (1999), Evolution of the North Caucasus foredeep: constraints based on the analysis of subsidence curves, *Tectonophysics*, *307*(3-4), 361-379, https://doi.org/10.1016/S0040-1951(99)00053-0.

Mikhailova, M. (2004), Water and sediment runoff at the mouths of rivers flowing into the Black Sea, *Environmental Research, Engineering and Management*, *48*, 5-10.

Milyukov, V., Kopaev, A., Zharov, V., Mironov, A., Myasnikov, A., Kaufman, M., & Duev, D. (2010), Monitoring crustal deformations in the Northern Caucasus using a high precision long base laser strainmeter and the GPS/GLONASS network, *Journal of Geodynamics*, *49*(3–4), 216-223, https://doi.org/10.1016/j.jog.2009.10.003.

Mosar, J., Kangarli, T., Bochud, M., Glasmacher, U. A., Rast, A., Brunet, M.-F., & Sosson, M. (2010), Cenozoic-Recent tectonics and uplift in the Greater Caucasus: a prespective from Azerbaijan, In M. Sosson, N. Kaymakci, R. A. Stephenson, F. Bergerat & V. Starostenko (Eds.), *Sedimentary basin tectonics from the Black Sea and Caucasus to the Arabian Platform*, (Vol. 340, pp. 261-280). London, Geological Society Special Publication.

Mouthereau, F. (2011), Timing of uplift in the Zagros belt/Iranian plateau and accommodation of late Cenozoic Arabia–Eurasia convergence, *Geological Magazine*, *148*(5-6), 726-738, doi: https://doi.org/10.1017/S0016756811000306.

Mumladze, T., Forte, A. M., Cowgill, E. S., Trexler, C. C., Niemi, N. A., Burak Yıkılmaz, M., & Kellogg, L. H. (2015), Subducted, detached, and torn slabs beneath the Greater Caucasus, *GeoResJ*, *5*, 36-46, https://doi.org/10.1016/j.grj.2014.09.004.

Murray, K. E., Braun, J., & Reiners, P. W. (2018), Toward Robust Interpretation of Low-Temperature Thermochronometers in Magmatic Terranes, *Geochemistry, Geophysics, Geosystems*, *19*, 3739-3763, https://doi.org/10.1029/2018GC007595.

Mutlu, A. K., & Karabulut, H. (2011), Anisotropic Pn tomography of Turkey and adjacent regions, *Geophysical Journal International*, *187*(3), 1743-1758, https://doi.org/10.1111/j.1365-246X.2011.05235.x.

Nikishin, A. M., Ziegler, P. A., Bolotov, S. N., & Fokin, P. A. (2012), Late Palaeozoic to Cenozoic evolution of the Black Sea-southern Eastern European region: a view from the Russian Platform, *Turkish Journal of Earth Sciences*, *21*(5), 571-634, https://doi.org/10.3906/yer-1005-22.

Norton, K., & Schlunegger, F. (2011), Migrating deformation in the central Andes from enhanced orographic rainfall. *Nature Communications*, 2, https://doi.org/10.1038/ncomms1590.

Palcu, D. V., Popov, S. V., Golovina, L. A., Kuiper, K. F., Liu, S., & Krijgsman, W. (2019), The shutdown of an anoxic giant: Magnetostratigraphic dating of the end of the Maikop Sea, *Gondwana Research*, *67*, 82-100, https://doi.org/10.1016/j.gr.2018.09.011.

Petrakov, D. A., Krylenko, I. V., Chernomorets, S. S., Tutubalina, O. V., Krylenko, I. N., & Shakhmina, M. S. (2007), Debris flow hazard of glacial lakes in the Central Caucasus, In C. L. Chen & J. J. Major (Eds.), *Debris-Flow Hazards Mitigation: Mechanics, Prediction, and Assessment*pp. 703-714). Netherlands, Millpress.

Philip, H., Cisternas, A., Gvishiani, A., & Gorshkov, A. (1989), The Caucasus: an actual example of the initial stages of continental collision, *Tectonophysics*, *161*, 1-21.

Polyak, B. G., Lavrushin, V. Y., & Kamensky, I. L. (2009), Mantle helium traces in the Elbrus–Kazbek sector of the Greater Caucasus and adjacent areas, *Chemical Geology*, *266*(1–2), 57-66, https://doi.org/10.1016/j.chemgeo.2008.08.005.

Polyak, B. G., Lavrushin, B. Y., Inguaggiato, S., & Kikvadze, O. E. (2011), Helium isotopes in gases of Mineral Waters in the western Caucasus, *Lithology and Mineral Resources*, *46*(6), 495-506506, https://doi.org/10.1134/s0024490211060113.

Polyak, B. G., Tolstikhin, I. N., Kamensky, I. L., Yakovlev, L. E., Cheshko, A. L., & Marty, B. (2000), Helium isotopes, tectonics and heat flow in the Northern Caucasus, *Geochimica et Cosmochimica Acta*, *64*(11), 1925-1944, https://doi.org/10.1016/s0016-7037(00)00342-2.

Reilinger, R., McClusky, S., Vernant, P., Lawrence, S., Ergintav, S., Cakmak, R. et al. (2006), GPS constraints on continental deformation in the Africa-Arabia-Eurasia continental collision zone and implications for the dynamics of plate interactions, *Journal of Geophysical Research*, *111*, B05411, https://doi.org/10.1029/2005JB004051.

Rets, E. P., Dzhamalov, R. G., Kireeva, M. B., Frolova, N. L., Durmanov, I. N., Telegina, A. A., Telegina, E. A., & Grigoriev, V. Y. (2018), Recent trends of river runoff in the North Caucasus. *Geography, Environment, Sustainability*, *11*(3), 61-70, https://doi.org/10.24057/2071-9388-2018-11-3-61-70.

Rezaeian, M., Carter, A., Hovius, N., & Allen, M. B. (2012), Cenozoic exhumation history of the Alborz Mountains, Iran: New constraints from low-temperature chronometry, *Tectonics*, *31*, https://doi.org/10.1029/2011tc002974.

Rogozhin, E. A., Gorbatikov, A. V., Kharazova, Y. V., Stepanova, M. Y., & Nikolaev, A. V. (2016), Deep structure and volcanic activity of Mount Elbrus and a portion of the Elbrus-Tyrnyauz valley: Geological and geophysical data, *Doklady Earth Sciences*, *471*(1), 1213-1216, https://doi.org/10.1134/s1028334x16110210.

Rolland, Y. (2017), Caucasus collisional history: Review of data from East Anatolia to West Iran, *Gondwana Research*, *49*, 130-146, doi: https://doi.org/10.1016/j.gr.2017.05.005.

Saintot, A., & Angelier, J. (2002), Tectonic paleostress fields and structural evolution of the NW-Caucasus fold-and-thrust belt from Late Cretaceous to Quaternary, *Tectonophysics*, *357*, 1-31, https://doi.org/10.1016/S0040-1951(02)00360-8.

Saintot, A., Brunet, M.-F., Yakovlev, F., Sébrier, M., Stephenson, R., Ershov, A., Chalot-Prat, F., & McCann, T. (2006a), The Mesozoic-Cenozoic tectonic evolution of the Greater Caucasus, In D. Gee & R. Stephenson (Eds.), *European Lithosphere Dynamics*, (Vol. 32, pp. 277-289), Geological Society, London, Memoir, https://doi.org/10.1144/GSL.MEM.2006.032.01.16.

Saintot, A., Stephenson, R., Stovba, S., Brunet, M.-F., Yegorova, T., & Starostenko, V. (2006b), The evolution of the southern margin of the Eastern Europe (Eastern European and Scythian platforms) from the latest Precambrian-Early Palaeozoic to the Early Cretaceous, In D. Gee & R. Stephenson (Eds.), *European Lithosphere Dynamics*, (Vol. 32, pp. 481-505), Geological Society, London, Memoir, https://doi.org/10.1144/GSL.MEM.2006.032.01.30.

Schildgen, T. F., van der Beek, P. A., Sinclair, H. D., & Thiede, R. C. (2018), Spatial correlation bias in late-Cenozoic erosion histories derived from thermochronology, *Nature*, *559*(7712), 89-93, https://doi.org/10.1038/s41586-018-0260-6.

Schwanghart, W., & Scherler, D. (2014), TopoToolbox 2 – MATLAB-based software for topographic analysis and modeling in Earth surface sciences, *Earth Surface Dynamics*, *2*, 1-7, https://doi.org/10.5194/esurf-2-1-2014.

Seinova, I.B., Andreev, Y. B., Krylenko, I. N., & Chernomorets, S. S., (2011), Regional short-term forecast of debris flow initiation for glaciated high mountain zone of the Caucasus, *Italian Journal of Engineering Geology and Environment*, *2011.3.B-109*, 1003-1011.

Snyder, N., Whipple, K., Tucker, G., & Merritts, D. (2000), Landscape response to tectonic forcing: digital elevation model analysis of stream profiles in the Mendocino triple junction region, Northern California, *Bulletin of the Geological Society of America*, *112*(8), 1250-1263.

Sobornov, K. O. (1994), Structure and petroleum potential of the Dagestan thrust belt, northeastern Caucasus, Russia, *Bulletin of Canadian Petroleum Geology*, *42*(3), 352-364.

Sokhadze, G., Floyd, M., Godoladze, T., King, R., Cowgill, E. S., Javakhishvili, Z., Hahubia, G., & Reilinger, R. (2018), Active convergence between the Lesser and Greater Caucasus in Georgia: Constraints on the tectonic evolution of the Lesser–Greater Caucasus continental collision, *Earth and Planetary Science Letters*, *481*, 154-161, https://doi.org/10.1016/j.epsl.2017.10.007.

Somin, M. (2011), Pre-Jurassic basement of the Greater Caucasus; brief overview, *Turkish Journal of Earth Sciences*, *20*(5), 545-610.

Somin, M. L. (2000), Structure of axial zones in the Central Caucasus, *Doklady Earth Sciences*, *375*(9), 1371-1374.

Sosson, M., Rolland, Y., Müller, C., Danelian, T., Melkonyan, R., Kekelia, S. et al. (2010), Subduction, obduction and collision in the Lesser Caucasus (Armenia, Azerbaijan, Georgia), new insights, In M. Sosson, N. Kaymakci, R. A. Stephenson, F. Bergerat & V. Starostenko (Eds.), *Sedimentary basin tectonics from the Black Sea and Caucasus to the Arabian Platform*, (Vol. 340, pp. 329-352), Geological Society, London, Special Publication, https://doi.org/10.1144/SP340.14.

Tari, G., Vakhania, D., Tatishvili, G., Mikeladze, V., Gogritchiani, K., Vacharadze, S. et al. (2018), Stratigraphy, structure and petroleum exploration play types of the Rioni Basin, Georgia, In M. D. Simmons, G. C. Tari & A. I. Okay (Eds.), *The Petroleum Geology of the Black Sea*, (Vol. 464, pp. 403-438). London, Geological Society, Special Publication, https://doi.org/10.1144/SP464.14.

Tibaldi, A., Alania, V., Bonali, F. L., Enukidze, O., Tsereteli, N., Kvavadze, N., & Varazanashvili, O. (2017a), Active inversion tectonics, simple shear folding and back-thrusting at Rioni Basin, Georgia, *Journal of Structural Geology*, *96*, 35-53, https://doi.org/10.1016/j.jsg.2017.01.005.

Tibaldi, A., Russo, E., Bonali, F. L., Alania, V., Chabukiani, A., Enukidze, O., & Tsereteli, N. (2017b), 3-D anatomy of an active fault-propagation fold: A multidisciplinary case study from Tsaishi, western Caucasus (Georgia), *Tectonophysics*, *717*, 253-269, https://doi.org/10.1016/j.tecto.2017.08.006.

Triep, E. G., Abers, G. A., Lerner-Lam, A. L., Mishatkin, V., Zakharchenko, N., & Starovoit, O. (1995), Active thrust fault of the Greater Caucasus: the April 29, 1991, Racha earthquake sequence and its tectonic implications, *Journal of Geophysical Research*, *100*(B3), 4011-4033.

Tutberidze, B. (2012), Cenozoic volcanism of the Caucasian mobile belt in Georgia, its geological-petrological peculiarities and geodynamics, *Turkish Journal of Earth Sciences*, *21*(5), 799-815.

van der Meer, D. G., van Hinsbergen, D. J. J., & Spakman, W. (2018), Atlas of the underworld: Slab remnants in the mantle, their sinking history, and a new outlook on lower mantle viscosity, *Tectonophysics*, *723*, 309-448, https://doi.org/10.1016/j.tecto.2017.10.004.

van Hunen, J., & Allen, M. B. (2011), Continental collision and slab break-off: A comparison of 3-D numerical models with observations, *Earth and Planetary Science Letters*, *302*(1-2), 27-37, https://doi.org/10.1016/j.epsl.2010.11.035.

Vezzoli, G., Garzanti, E., Vincent, S. J., Andò, S., Carter, A., & Resentini, A. (2014), Tracking sediment provenance and erosional evolution of the western Greater Caucasus, *Earth Surface Processes and Landforms*, *39*(8), 1101-1114, https://doi.org/10.1002/esp.3567.

Vincent, S. J., Braham, W., Lavrishchev, V. A., Maynard, J. R., & Harland, M. (2016), The formation and inversion of the western Greater Caucasus Basin and the uplift of the western Greater Caucasus: Implications for the wider Black Sea region, *Tectonics*, *35*, 2948-2962, https://doi.org/10.1002/2016TC004204.

Vincent, S. J., Carter, A., & Somin, M. L. Pangaea data repository citation.

Vincent, S. J., Carter, A., Lavrishchev, V. A., Rice, S. P., Barabadze, T. G., & Hovius, N. (2011), The exhumation of the western Greater Caucasus: a thermochronometric study, *Geological Magazine*, *148*(1), 1-21, https://doi.org/10.1017/S0016756810000257.

Vincent, S. J., Morton, A. C., Carter, A., Gibbs, S., & Barabadze, T. G. (2007), Oligocene uplift of the Western Greater Caucasus; an effect of initial Arabia-Eurasia collision, *Terra Nova*, *19*, 160-166, https://doi.org/10.1111/j.1365-3121.2007.00731.x.

Vincent, S. J., Saintot, A., Mosar, J., Okay, A. I., & Nikishin, A. M. (2018), Comment on "Relict basin closure and crustal shortening budgets during continental collision: An example from Caucasus sediment provenance" by Cowgill et al. (2016), *Tectonics*, *37*(3), 1006-1016.

Weatherall, P., Marks, K.M., Jakobsson, M., Schmitt, T., Tani, S., Arndt, J.E., Rovere, M., Chayes, D., Ferrini, V., & Wigley, R., (2015), A new digital bathymetric model of the world's oceans. *Earth and Space Science*, *2*(8), 331-345, https://doi.org/10.1002/2015EA000107

Westaway, R. (1994), Present-day kinematics of the Middle East and eastern Mediterranean, *Journal of Geophysical Research: Solid Earth*, *99*(B6), 12071-12090, doi: 10.1029/94JB00335.

Whipple, K. X. (2004), Bedrock rivers and the geomorphology of active orogens, *Annual Review of Earth and Planetary Sciences*, *32*, 151-185, https://doi.org/10.1146/annurev.earth.32.101802.120356.

Whipple, K. X. (2009), The influence of climate on the tectonic evolution of mountain belts (vol 2, 97-104, 2009), *Nature Geoscience*, *2*(10), 730, https://doi.org/10.1038/ngeo638.

Whipple, K. X., & Meade, B. J. (2006), Orogen response to changes in climatic and tectonic forcing, *Earth and Planetary Science Letters*, *243*(1-2), 218-228, https://doi.org/10.1016/j.epsl.2005.12.022.

Wobus, C., Whipple, K. X., Kirby, E., Snyder, N., Johnson, J., Spyropolou, K., Crosby, B., & Sheehan, D. (2006), Tectonics from topography: procedures, promise, and pitfalls, In S. D. Willett, N. Hovius, M. T. Brandon & D. M. Fisher (Eds.), *Tectonics, Climate, and Landscape Evolution*, (Vol. 398, pp. 55-74), Geological Society of America Special Paper.

Zabelina, I., Koulakov, I., Amanatashvili, I., El Khrepy, S., & Al-Arifi, N. (2016), Seismic structure of the crust and uppermost mantle beneath Caucasus based on regional earthquake tomography, *Journal of Asian Earth Sciences*, *119*, 87-99, http://dx.doi.org/10.1016/j.jseaes.2016.01.010.

Zor, E. (2008), Tomographic evidence of slab detachment beneath eastern Turkey and the Caucasus, *Geophysical Journal International*, *175*, 1273-1282.

Sample No	Position (derived from)		Location	Lithology	Age (U-Pb; Ma)	Approx. altitude (m)	Analyses
	Latitude (N)	Longitude (E)					
MS_002_1	43.322625	42.7748305	Baksan R	Gneiss		1585	AFT
MS_002_24	43.3559305	42.7348388	Kyrtyk R	Orthogneiss		2160	AFT
MS_002_50	43.7195705 (~43.705803)	40.8393646 (~40.829514)	Bolshaya Laba R	Eclogite (boulder)		1125 1135	AFT, AHe
MS_002_51	43.7197326 (~43.705804)	40.8391322 (~40.829515)	Bolshaya Laba R	Gneissic aplite dike (boulder)		1130 1135	AFT, AHe
MS_003_29	43.4465277	41.4786972	Aksaut R	Migmatite leucosome		1700	AFT
MS_004_3	43.3507277	42.8323138	Mukulan stream, Baksan basin	Metagranite	305±8	2280	AFT, ZFT
MS_004_4	43.2665472	42.4367138	Baksan R	Orthogneiss		2880	AFT
MS_004_42c	43.4843916	41.2368583	Sophia R	Metagranite		2005	AFT
MS_008_1	43.3263777	42.8323138	Baksan R	Metagranite		1880	AFT
MS_011_1	43.3561916	42.7346972	Kyrtyk R	Amphibolite	425±9	2170	AFT
MS_015_1	43.2665444	42.4777583	Baksan R	Orthogneiss		2380	AFT, ZFT
MS_029_1	43.3559305	42.7348388	Kyrtyk R	Mica schist		2160	AFT
MS_040_1	43.7701916	40.8580694	Bolshaya Laba R	Orthogneiss	385±10	1050	AFT, AHe
MS_047_1	43.9333361	40.8592722	Bolshaya Laba R	Orthogneiss	388±10	1300	AFT
MS_078_1	43.4608306 (~43.397709)	41.1649833 (~41.18801)	Psysh R	Orthogneiss (boulder)		1690 2230	AFT
MS_092_1	43.1060000 (~43.10027)	43.1327900 (~43.13141)	Ulluchiran glacier	Orthogneiss (colluvial block)		2190 2385	AFT, ZFT
MS_093_1	43.1072833 (~43.12000)	43.1310027 (~43.10551)	Ulluchiran glacier	Orthogneiss (colluvial block)		2200 3730	AFT, ZFT
MS_098_1	43.1135400 (~43.11144)	43.1428000 (~43.13623)	Ulluchiran glacier	Orthogneiss (colluvial block)		2090 2220	AFT
MS_146_1	43.6336055	40.7956972	Damkhurts R	Amphibolite	454±10	1985	AFT, AHe
WC147/2	43.7039 (~43.74713)	40.2706 (~40.35187)	Laura R	Gneiss (boulder)		585 1455	AHe

Table 1. Details of the thermochronometric samples analysed in this study. Sample positions in parenthesis are the locations from which colluvial / fluvial boulder samples are thought to have been derived. These positions are plotted on all maps and graphs.

Sample No	Analysis	No of crystals	Track densities are (x10^6 tr cm^{-2}) Dosimeter		Spontaneous		Induced		Age dispersion		Central age	Mean track	SD	No of
			ρd	Nd	ρs	Ns	ρi	Ni	$P\chi^2$	RE%	(Ma±1σ)	length (μm)		tracks
MS_002_1	AFT	30	1.010	5599	0.019	43	1.069	2278	96.7	0.1	3.2±0.5	13.63±0.25	0.35	2
MS_002_24	AFT	30	1.010	5599	0.010	32	0.093	2155	17.8	58.1	2.4±0.5			
MS_002_50	AFT	20	1.010	5599	0.265	527	0.934	1858	65.9	0.4	48.2±2.5	13.98±0.19	1.29	43
MS_002_51	AFT	16	1.010	5599	0.307	306	2.124	2118	83.6	0.2	24.6±1.5	12.43±0.59	1.58	7
MS_003_29	AFT	20	1.010	5599	0.629	300	4.776	2312	8.1	16.3	22.3±1.6	12.95±0.53	2.62	24
MS_004_3	AFT	30	1.010	5599	0.022	45	2.642	5599	24.9	45.8	1.4±0.2			
MS_004_4	AFT	20	1.010	5599	0.151	167	3.520	4127	23.6	18.1	7.0±0.6			
MS_004_42c	AFT	16	1.010	5599	0.138	89	1.265	828	31.9	16.3	18.2±2.2			
MS_008_1	AFT	30	1.010	5599	0.031	35	6.538	734	98.3	0.0	8.1±1.4			
MS_011_1	AFT	30	1.010	5599	0.023	31	1.439	2095	11.2	3.8	2.5±0.5			
MS_015_1	AFT	26	1.010	5599	0.036	40	1.319	1444	95.4	0.1	4.7±0.8			
MS_029_1	AFT	20	1.010	5599	0.054	66	1.250	1619	36.9	17.5	7.0±0.9			
MS_040_1	AFT	19	1.010	5599	0.079	58	0.300	214	99.2	0.0	46.1±6.9			
MS_043_1	AFT		1.010	5599							Low uppm	bad mica		
MS_047_1	AFT	20	1.010	5599	1.415	159	8.165	988	41.8	7.7	27.6±7.7	11.84±0.36	2.32	11
MS_078_1	AFT	25	1.010	5599	0.135	96	2.927	2116	36.5	13.2	7.7±0.8	13.22±0.29	1.65	33
MS_092_1	AFT	20	1.010	5599	0.142	136	6.175	5962	67.9	2.0	3.9±0.3	12.71±0.37	2.05	30
MS_093_1	AFT	20	1.010	5599	0.096	75	5.578	4234	98.8	0.0	3.0±0.4			
MS_098_1	AFT	20	1.010	5599	0.154	224	3.432	5130	85.8	0.1	7.4±0.5	13.81±1.02	1.76	3
MS_146_1	AFT	11	1.010	5599	0.004	30	0.245	194	88.9	0.0	26.3±5.2			
MS_004_3	ZFT	14	0.547	3794	2.817	88	5.856	1849	10.6	26.0	1.7±0.2			
MS_015_1	ZFT	6	0.547	3794	2.184	220	3.110	327	10.0	10.1	231.6±17.2			
MS_092_1	ZFT	11	0.547	3794	20.59	2674	5.814	771	0.07	18.1	120.3±8.4			
MS_093_1	ZFT	14	0.547	3794	23.04	2005	6.786	587	28.5	2.6	117.6±6.0			

Analyses by external detector method using 0.5 for the $4\pi/2\pi$ geometry correction factor;
Ages calculated using dosimeter glass CN-5; (apatite) ζ_{CN5} =339±5; calibrated by multiple analyses of IUGS apatite and zircon age standards (see Hurford 1990);
$P\chi^2$ is probability for obtaining χ^2 value for v degrees of freedom, where v = no. crystals - 1;
Central age is a modal age, weighted for different precisions of individual crystals (see Galbraith & Laslett, 1993)

Table 2. Apatite and zircon fission track results.

Sample No.	^{4}He (ncc)	U (ppm)	Th (ppm)	Sm (ppm)	Th/U ratio (atomic)	Grain Length (μm)	Grain width (μm)	R* (μm)	F_T	Raw Age (Ma)	Corrected Age (Ma)	Error (±1σ)	[eU]
MS_002_50A	0.183	12.1	99.0	1418.2	0.13	85	68	36.4	0.59	14.2	24.0	1.68	101.8
MS_002_50B	0.185	25.6	86.3	1366.4	0.30	99	62	35.4	0.58	16.2	28.1	1.96	92.4
MS_002_50D	0.594	13.4	143.5	1048.2	0.10	142	79	46.4	0.68	14.6	21.5	1.51	146.7
MS_002_50E	0.623	11.7	137.3	1548.0	0.09	116	85	46.7	0.68	16.6	24.4	1.71	140.1
Mean (s.d.)										15.4 (1.2)	24.5 (2.7)		
MS_002_51A	0.09	20.0	27.0	1087.0	0.76	128	77	44.4	0.62	10.0	15.1	1.06	31.7
MS_002_51B	0.28	85.2	43.8	138.9	1.99	141	79	46.3	0.67	16.5	24.8	1.73	63.9
MS_002_51C	0.11	2.1	36.8	103.6	0.06	156	83	49.2	0.70	9.1	13.0	0.91	37.3
MS_040_1a	0.004	1.7	0.9	3.5	1.86	131	97	53.1	0.71	8.2	11.6	0.81	1.3
MS_040_1b	0.010	0.4	0.8	2.0	0.56	161	146	75.3	0.80	10.1	12.6	0.88	0.9
MS_040_1c	0.007	0.2	0.2	2.0	1.05	204	196	99.3	0.85	11.6	13.7	0.96	0.2
Mean (s.d.)										10.0 (1.7)	12.6 (1.1)		
MS_146_1A	0.012	8.2	5.0	52.5	1.70	194	92	55.8	0.72	3.4	4.7	0.33	6.9
MS_146_1C	0.014	1.2	5.3	61.7	0.24	141	118	62.4	0.76	4.0	5.3	0.37	5.6
MS_146_1D	0.017	1.0	5.5	45.2	0.19	164	115	63.9	0.77	4.4	5.8	0.40	5.7
MS_146_1E	0.020	0.9	5.8	65.0	0.16	146	121	64.2	0.77	4.9	6.3	0.44	6.1
MS_146_1F	0.007	1.5	3.4	52.9	0.45	172	91	54.0	0.72	4.3	5.9	0.42	3.7
Mean (s.d)										4.2 (0.5)	5.6 (0.6)		
WC147_2A	0.271	14.6	60.6	60.9	0.25	171	86	51.5	0.71	11.0	15.5	1.09	64.1
WC147_2B	0.329	20.9	65.0	81.8	0.33	155	86	50.5	0.70	13.5	19.2	1.34	69.9
WC147_2C	0.314	22.0	110.2	112.3	0.20	125	74	42.8	0.65	13.1	20.1	1.41	115.3
WC147_2D	0.223	51.8	107.6	599.4	0.49	136	78	45.5	0.67	7.3	10.9	0.76	119.8
WC147_2E	0.197	11.3	105.5	103.5	0.11	122	74	42.6	0.65	9.0	13.8	0.97	108.2
WC147_2G	0.205	24.6	110.7	120.6	0.23	132	70	41.5	0.64	9.0	14.0	0.98	116.4
WC147_2H	0.160	7.0	52.3	65.5	0.14	135	77	44.9	0.67	12.2	18.3	1.28	53.9

Table 3. Apatite (U-Th)/He dating results. Replicates are omitted that outgassed strangely or where grains or packets were lost during retrieval from the helium line and placing in vials for dissolution. Average ages are only shown where samples have similar radius and eU values and show < 20% age dispersion. Raw ages are used in the modelling and are cited in the text. R* = spherical equivalent radius calculated as **R*** = (3 * (**RL**))/(2 * (**R** + **L**)), where **R** =**W**/2.

	Average sector AFT cooling age (Ma) [this study; Avdeev and Niemi, 2011; Král and Gurbanov, 1996; Vincent et al., 2011]	Average sector exhumation rate (mm a^{-1}) assuming a 40°C km^{-1} geothermal gradient [this study; Avdeev and Niemi, 2011; Král and Gurbanov, 1996; Vincent et al., 2011]	Average erosion rate from modern catchments (mm a^{-1}) [this study; Vezzoli et al., 2014]	Average normalized bedrock channel channel-steepness index (k_{sn}) (this study)
NW	32.5 (n=37)	0.10 (1)	Kuban: 0.05±0.02 (1)	81±11 (1)
NE	6.3 (n=35)	0.45 (4.5)	Baksan: 0.26±0.12(4.9)	140±20 (1.7)
SW	-	-	Mzimta: 0.16±0.08 (2.9)	120±40 (1.5)
SE	2.5 (n=1)	0.90 (9.0)	Inguri & Rioni: 0.26±0.09 (4.9)	137±21 (1.7)

Table 4. Average exhumation and uplift proxies for the four sectors of the western Greater Caucasus as delineated in Figures 2 and 12. Values normalized to the north-western sector are shown in parentheses. Named rivers are highlighted on Figure 12.

Figure 1. Shaded relief DEM of the Arabia-Eurasia collision zone showing selected GPS-constrained motions relative to stable Eurasia, the occurrence of instrumentally recorded earthquakes (M ≥ 4.5) and a selected number of their focal mechanisms. The grey box locates the study area, the red boxes the sampling sites of Avdeev [2011] and Bochud [2017]. The white lines are Neo-Tethyan sutures and the black line is a transect along which strike parallel data are located as presented in Figure 6. The GPS motions are coloured according to geologic position and are taken from Reilinger et al. [2006], Karakhanyan et al.

[2013] and Sokhadze et al. [2018]. The focal mechanisms are from Copley and Jackson [2006]. The seismicity record is taken from the US National Earthquake Information Center catalogue (1973-June 2009), the Centennial Earthquake Catalog [Engdahl and Villaseñor, 2002] and Jackson (2014, *pers. comm.*). The crystalline crustal thickness north of the Caucasus is adapted from Saintot et al. [2006b] [after Kostyuchenko et al., 2004].

Figure 2. Simplified geological map of the western Greater Caucasus based on Soviet and Russian 1:500,000 and 1:200,000 geological maps draped on a hillshaded DEM. All thermochronometric sample positions are shown, with those new to this study labelled. The rivers analysed in this study are also labelled. The dashed blue lines form the outlines of the four sectors of the range described in the text. Additional data on the Miocene and younger magmatic centers are given in Table S1. The Racha earthquake focal mechanism is from Triep et al. [1995]. Note that the position of the Main Caucasus Thrust, at the southern margin of the crystalline core of the range, as defined by the likes of Dotduyev [1986], Mosar et al. [2010] and Somin et al. [2011], differs from that of Sokhadze et al. [2018].

Figure 3. Schematic cross section through the western Greater Caucasus between Mt. Elbrus and Mt. Kazbek (see Figure 2 for location). The cross section is adapted from Vincent et al. [2018] and based upon the surface geology of Dzhanelidze and Kandelaki [1955], Melnikov and Popova [1966] and Somin [2000]. With the exception of the plane defined by Racha earthquake aftershocks [Fuenzalida et al., 1997], geological structures at depth are highly speculative and are influenced by the interpretations of Dotduyev [1986], Triep et al. [1995] and Banks et al. [1997].

Figure 4. Shaded relief DEM of the Arabia-Eurasia collision zone showing the main plate boundaries and their interactions as proposed by Reilinger et al. (2006). Double white lines

are extensional plate boundaries, plain lines are strike-slip boundaries and lines with triangular tick marks are compressional (thrust) boundaries. Dark numbers are GPS-derived slip rates (mm a^{-1}) on block bounding faults (those in parenthesis are strike slip). White arrows and figures are GPS-derived plate velocities (mm a^{-1}) relative to Eurasia. Curved arrows show the sense of block rotations relative to Eurasia. Note that the study area (highlighted in the white box) is considered to form part of stable Eurasia at the present day. The main folds (blue) and faults (red) in the region are also shown and are extended from Allen et al. [2003]. The Elbrus and Kazbek volcanic centres are shown as yellow stars. Abbreviations: AS - Apsheron sill; AT - Adjara-Trialet belt; EBS - Eastern Black Sea; EGC – eastern Greater Caucasus; PT - Pontides; SCB - South Caspian Basin; T - Talysh; TA - Taurides-Anatolides; TC - Transcaucasus; WBS - Western Black Sea; WGC – western Greater Caucasus.

Figure 5. Simplified geological map of the western Greater Caucasus (see Figure 2 for a more legible version of the text) with various data overlays. Note that in parts a-c thermochronometric sample sizes symbolize a relative measure of exhumation rate as they are inversely proportional to their cooling age (i.e. the younger the cooling age the larger the symbol). (a) AFT and cosmogenic nuclide (with associated catchment area) results from previous studies. The cosmogenic nuclide sample size is based on a conversion of erosion rate to equivalent AFT cooling age. (b) AFT and AHe results from this study. Given the lower closure temperature of the AHe system, the exhumation rate implications of these two data sets are not equivalent. (c) ZFT analysis results from this and previous studies. Note the different symbol scale. (d) $^{3}He/^{4}He$ isotopic values of subsurface fluids from Polyak et al. [2009; 2011; 2000] and sources therein and the location of Middle Miocene and younger volcanic centers. Note the marked decrease in AFT ages to the east of Mt. Elbrus in all the FT data sets and the broad coincidence of young AFT ages with the volcanic centres and high

concentrations of mantle-derived helium. The anomalously young cooling ages of sample MS_004_03 (this study) and sample 228C [Král and Gurbanov, 1996] are omitted from these plots (see Figure 6).

Figure 6. Plot of thermochronometric cooling ages and subsurface fluid $^3He/^4He$ values versus western Greater Caucasus strike-parallel distance (N110E). Note the increase in AFT ages and decrease in He values (away from its MORB value) to the west of Mt. Elbrus. The ages of the samples with the youngest AFT and ZFT ages in this study and the youngest AFT age in the study of Kral and Gurbanov [1996] should be treated with caution as they may have undergone thermal overprinting of their exhumation ages due to the emplacement of nearby magmatic bodies.

Figure 7. Alternative models for zones of possible rapid Pliocene uplift within the western Greater Caucasus as proposed by Vincent et al. [2011]. The findings of this study are consistent with model 2. See Figure 2 for more details of the background geological map.

Figure 8. Plot of thermochronometric cooling age versus western Greater Caucasus strike-perpendicular distance (N020E) relative to the Main Caucasus Thrust west (a) and east (b) of Mt. Elbrus. Note the increase in fission track ages in the footwall of the Racha-Lechkumi fault and the similarity in ages on either side of the Main Caucasus Thrust to the east of Mt. Elbrus. The ages of the samples with the youngest AFT and ZFT ages in this study and the youngest AFT age in the study of Kral and Gurbanov [1996] should be treated with caution as they may have undergone thermal overprinting of their exhumation ages due to the emplacement of nearby magmatic bodies.

Figure 9. Selected best-fit thermal models for AFT samples from the north-western sector of the western Greater Caucasus. These were modelled using QTQt [Gallagher, 2012] where

1000 good thermal paths were obtained. Sample locations are shown on Figure 2. The blue line corresponds to the most probable thermal history and the purple lines encompass the 2σ confidence limits. The AFT data for sample WC147/2 were taken from Vincent et al. [2011].

Figure 10. Exhumation rate history of the western Greater Caucasus inferred from the linear inversion of thermochronometric data. Data points are marked as black dots. The exhumation rate outputs (left hand views) are cropped to 800 m asl. The resolution values (right hand outputs) give a guide to the confidence of the exhumation rate model time interval, where 1 is when the data constrain the exhumation rate independently of the prior rate and rates in other time steps. The beginning of successive time intervals are defined by the (a) base Oligocene / Maykop, (b) base Miocene, (c) top Maykop, (d) base late Sarmatian, (e) base Pliocene. The Maykop and Sarmatian terms are Eastern Paratethyan stage names adopted regionally because of the semi-isolation of the Black Sea / Greater Caucasus region from the global ocean from the Oligocene onwards [see Jones and Simmons, 1997]. The age of the top of the Paratethyan Maykop stage is defined by Palcu et al. [2019]; other ages are from Gradstein et al. [2012]. Input parameters are as stated in the text. Note (1) the discrete region of rapid exhumation between Mt. Elbrus and Mt. Kazbek during the 5.33-0 Ma time interval, and (2) the suppressed exhumation rates in broadly the same region during the preceding time interval as a consequence of the modelling procedure (cf. Figure 11b, and the text for details).

Figure 11. Alternative exhumation rate maps of the linear inversion of thermochronometric data from the western Greater Caucasus to illustrate specific scenarios. (a-b) The recalculation of the last two steps of the linear inversion model with Pliocene and younger

thermochronometric cooling ages excluded. This scenario is an end-member example assuming all Pliocene and younger cooling is a result of magmatic rather than exhumational cooling. (c) The Pliocene to present day interval with an enhanced present day geothermal gradient of 60°C. Note how this suppresses the exhumation rates in the Mt. Elbrus to Mt. Kazbek region to values similar to those farther to the west when a 38°C present day geothermal gradient is used (Figure 10a). Further input parameters are as stated in the text. Additional information are given in the caption to Figure 10.

Figure 12. Map of normalized channel-steepness indices for rivers draining the western Greater Caucasus. The dashed lines show the extent of the four sectors discussed in the text and their average k_{sn} values. The names of rivers with erosion rate data (Table 4) are highlighted in yellow. The box shows the locations of active structures around Suchumi (Figure 13). See Figure 2 for the key to the colour version of the background geological map.

Figure 13. False colour Landsat 7 image of the interaction of drainage systems and active structures in the Suchumi region of Abkhazia. Note the drainage deflection around the western tip of the northernmost pericline and the wind gaps due to channel abandonment in the southern two periclines. See Figure 12 for location.

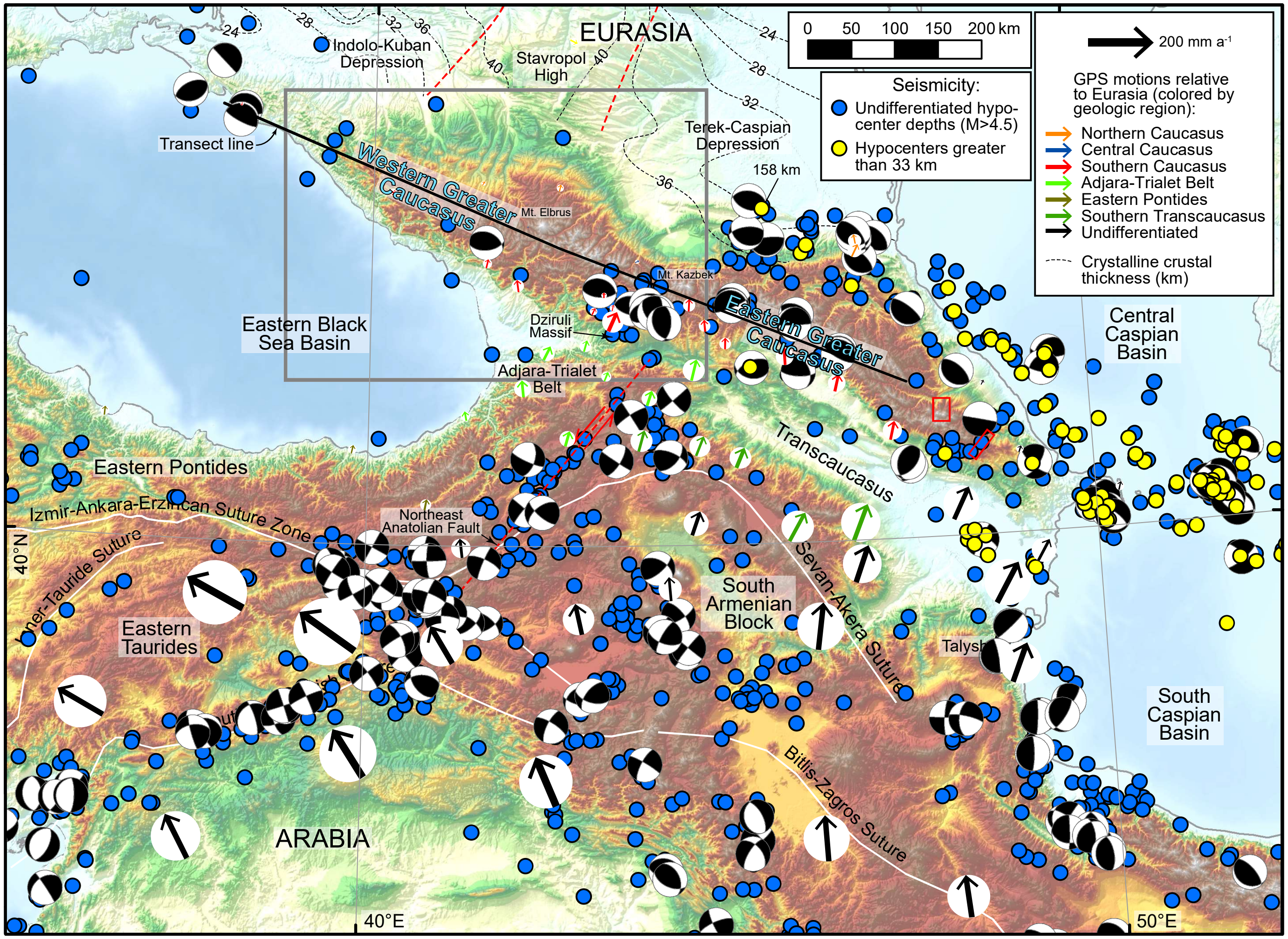

EURASIA
Indolo-Kuban Depression
Stavropol High
Terek-Caspian Depression
Transect line
Western Greater Caucasus
Mt. Elbrus
Mt. Kazbek
Eastern Greater Caucasus
Eastern Black Sea Basin
Dziruli Massif
Adjara-Trialet Belt
Eastern Pontides
Izmir-Ankara-Erzincan Suture Zone
Northeast Anatolian Fault
Transcaucasus
Sevan-Akera Suture
South Armenian Block
Eastern Taurides
Bitlis-Zagros Suture
ARABIA
Talysh
Central Caspian Basin
South Caspian Basin
158 km
40°N
40°E
50°E
0 50 100 150 200 km
Seismicity:
Undifferentiated hypocenter depths (M>4.5)
Hypocenters greater than 33 km
200 mm a-1
GPS motions relative to Eurasia (colored by geologic region):
Northern Caucasus
Central Caucasus
Southern Caucasus
Adjara-Trialet Belt
Eastern Pontides
Southern Transcaucasus
Undifferentiated
Crystalline crustal thickness (km)

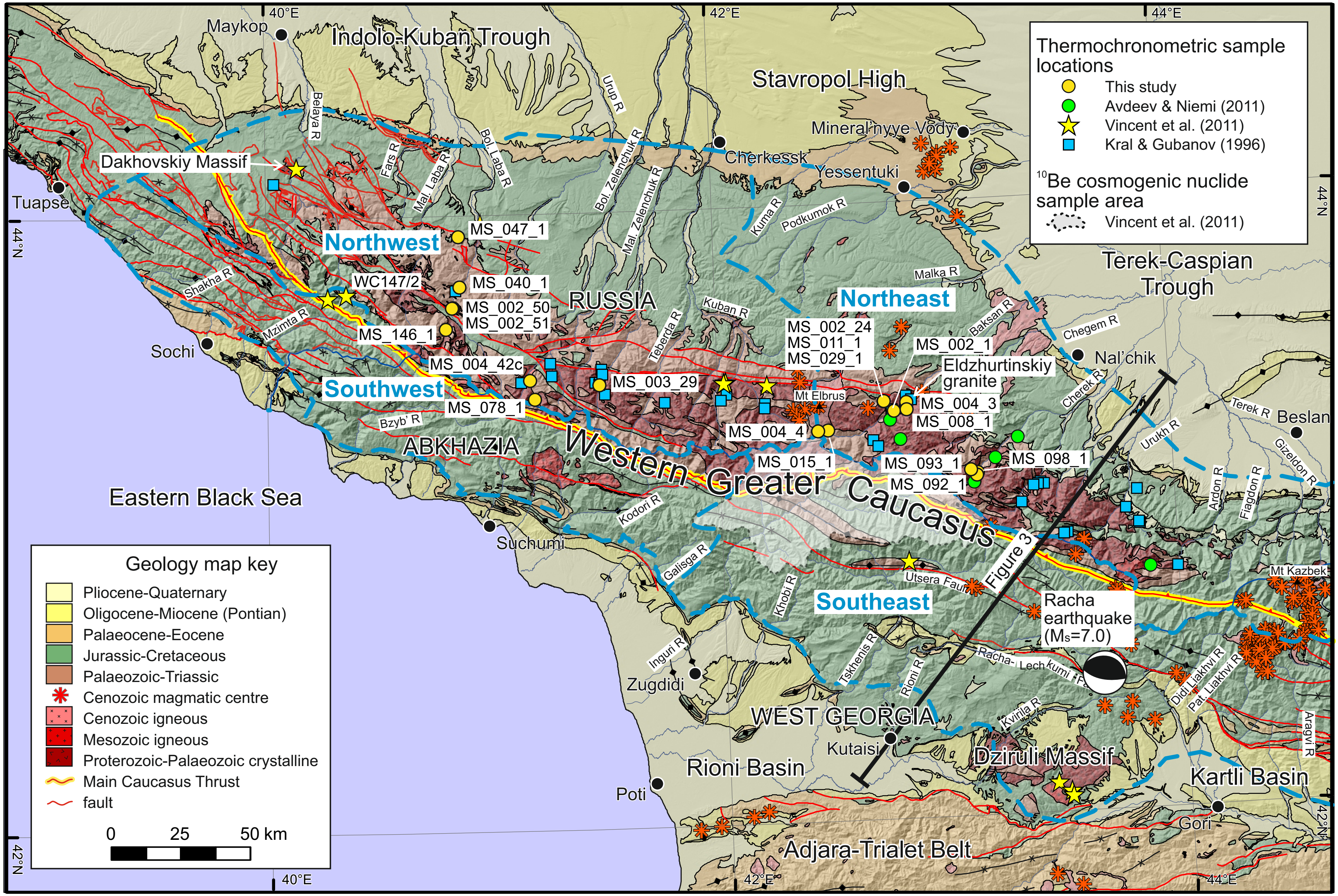

Indolo-Kuban Trough
Stavropol High
Terek-Caspian Trough
Thermochronometric sample locations
This study
Avdeev & Niemi (2011)
Vincent et al. (2011)
Kral & Gubanov (1996)
10Be cosmogenic nuclide sample area
Vincent et al. (2011)
Maykop
Tuapse
Sochi
Suchumi
Zugdidi
Kutaisi
Poti
Gori
Nal'chik
Beslan
Cherkessk
Yessentuki
Mineral'nyye Vody
Dakhovskiy Massif
Northwest
Northeast
Southwest
Southeast
RUSSIA
ABKHAZIA
WEST GEORGIA
Western Greater Caucasus
Eastern Black Sea
Rioni Basin
Kartli Basin
Dziruli Massif
Adjara-Trialet Belt
Mt Elbrus
Mt Kazbek
Eldzhurtinskiy granite
Racha earthquake (Ms=7.0)
Utsera Fault
Racha-Lechkumi F.
Figure 3
MS_047_1
MS_040_1
WC147/2
MS_002_50
MS_002_51
MS_146_1
MS_004_42c
MS_078_1
MS_003_29
MS_002_24
MS_011_1
MS_029_1
MS_002_1
MS_004_3
MS_008_1
MS_004_4
MS_015_1
MS_093_1
MS_092_1
MS_098_1
Belaya R
Fars R
Mal. Laba R
Bol. Laba R
Urup R
Bol. Zelenchuk R
Mal. Zelenchuk R
Kuma R
Podkumok R
Malka R
Baksan R
Chegem R
Cherek R
Urukh R
Terek R
Gizeldon R
Ardon R
Fiagdon R
Kuban R
Teberda R
Shakha R
Mzimta R
Bzyb' R
Kodori R
Galisga R
Khobi R
Inguri R
Tskhenis R
Rioni R
Kvirila R
Didi Liakhvi R
Pat. Liakhvi R
Aragvi R
40°E
42°E
44°E
44°N
42°N
Geology map key
Pliocene-Quaternary
Oligocene-Miocene (Pontian)
Palaeocene-Eocene
Jurassic-Cretaceous
Palaeozoic-Triassic
Cenozoic magmatic centre
Cenozoic igneous
Mesozoic igneous
Proterozoic-Palaeozoic crystalline
Main Caucasus Thrust
fault
0 25 50 km

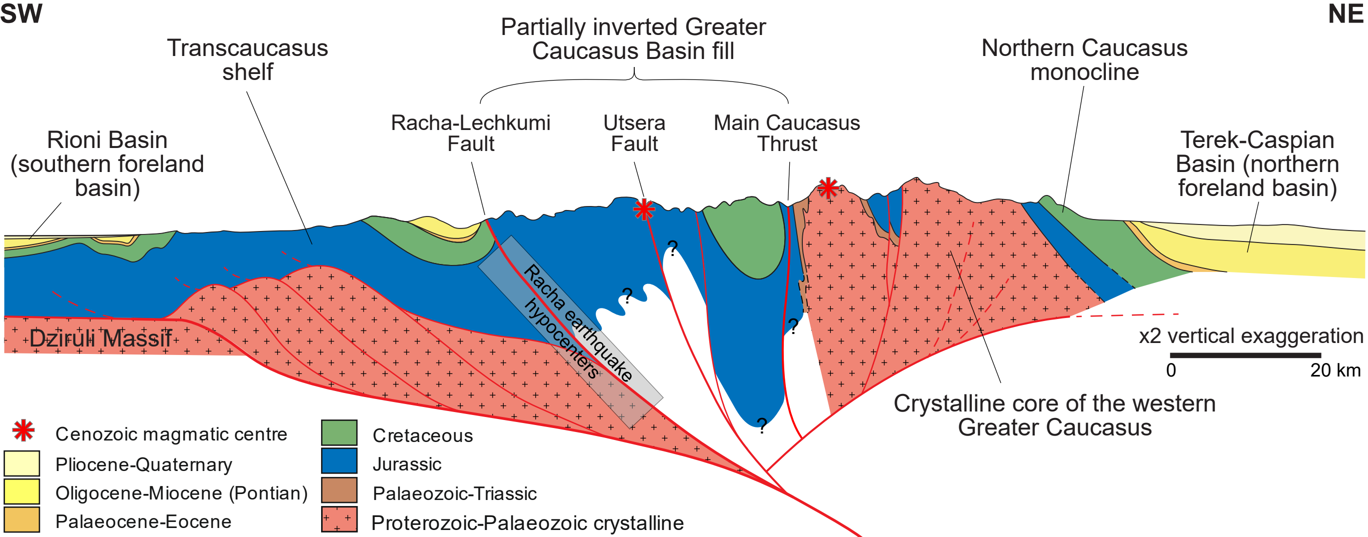
SW
NE
Partially inverted Greater Caucasus Basin fill
Transcaucasus shelf
Northern Caucasus monocline
Rioni Basin (southern foreland basin)
Racha-Lechkumi Fault
Utsera Fault
Main Caucasus Thrust
Terek-Caspian Basin (northern foreland basin)
Racha earthquake hypocenters
Dziruli Massif
x2 vertical exaggeration
0
20 km
Crystalline core of the western Greater Caucasus
?
Cenozoic magmatic centre
Pliocene-Quaternary
Oligocene-Miocene (Pontian)
Palaeocene-Eocene
Cretaceous
Jurassic
Palaeozoic-Triassic
Proterozoic-Palaeozoic crystalline

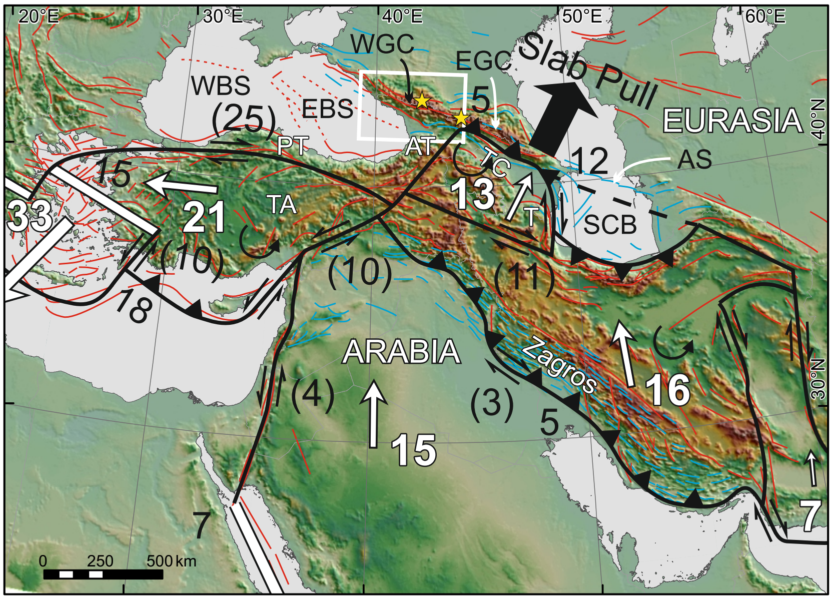
20°E
30°E
40°E
50°E
60°E
40°N
30°N
WGC
EGC
Slab Pull
WBS
EBS
(25)
PT
AT
5
EURASIA
12
AS
15
13
TC
T
33
21
TA
SCB
(10)
(10)
(11)
18
ARABIA
Zagros
16
(4)
(3)
5
15
7
7
0
250
500 km

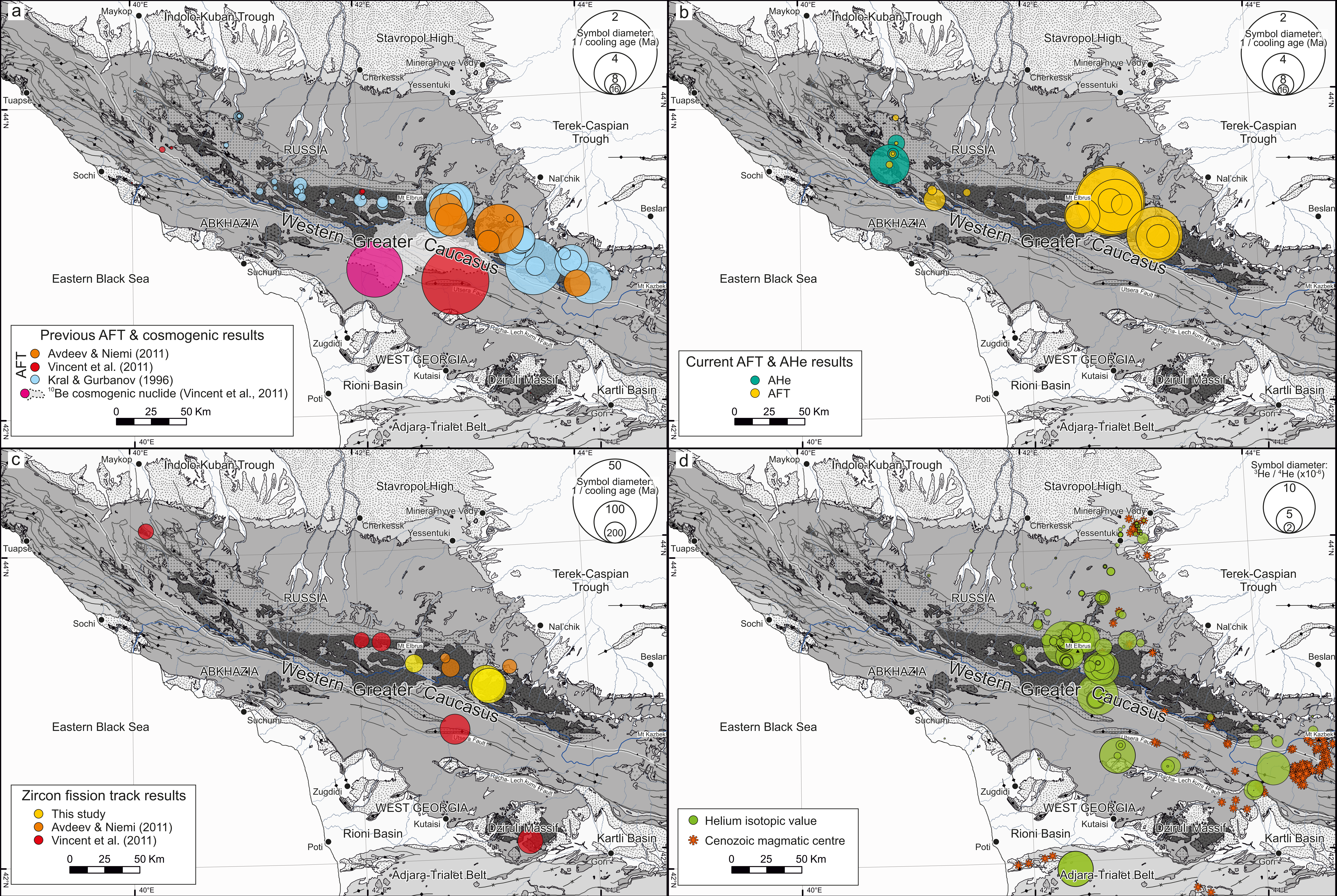

a
b
c
d
Maykop
Indolo-Kuban Trough
Stavropol High
Mineral'nyye Vody
Cherkessk
Yessentuki
Tuapse
Terek-Caspian Trough
RUSSIA
Sochi
Nal'chik
Beslan
Mt Elbrus
ABKHAZIA
Western Greater Caucasus
Eastern Black Sea
Suchumi
Mt Kazbek
Utsera Fault
Racha- Lech kumi Fault
Zugdidi
WEST GEORGIA
Kutaisi
Rioni Basin
Dziruli Massif
Kartli Basin
Poti
Gori
Adjara-Trialet Belt
40°E
42°E
44°E
44°N
42°N
Symbol diameter: 1 / cooling age (Ma)
2
4
8
16
50
100
200
Symbol diameter: ^3He / ^4He (x10^{-6})
10
5
2
Previous AFT & cosmogenic results
AFT
Avdeev & Niemi (2011)
Vincent et al. (2011)
Kral & Gurbanov (1996)
^{10}Be cosmogenic nuclide (Vincent et al., 2011)
Current AFT & AHe results
AHe
AFT
Zircon fission track results
This study
Avdeev & Niemi (2011)
Vincent et al. (2011)
Helium isotopic value
Cenozoic magmatic centre
0 25 50 Km

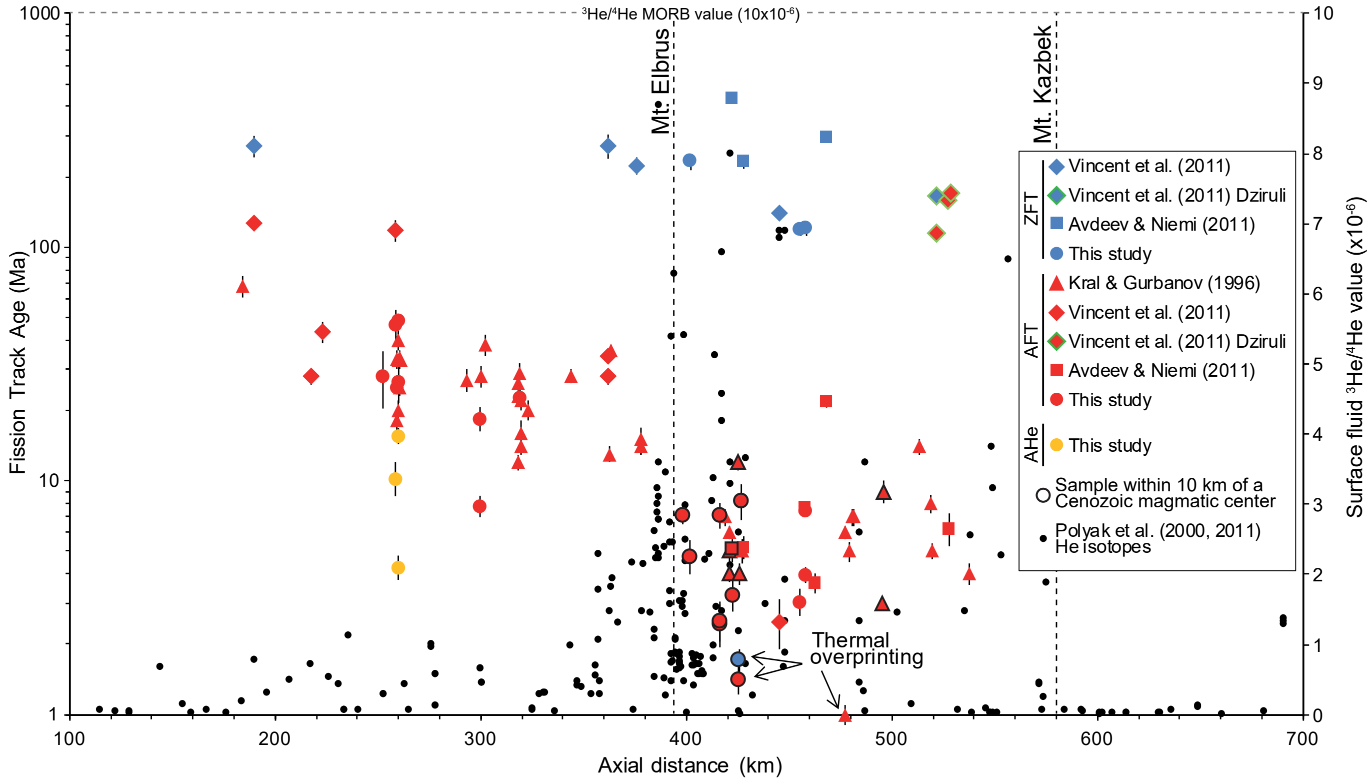

1000
100
10
1
Fission Track Age (Ma)
100
200
300
400
500
600
700
Axial distance (km)
Surface fluid 3He/4He value (x10-6)
3He/4He MORB value (10x10-6)
Mt. Elbrus
Mt. Kazbek
ZFT
Vincent et al. (2011)
Vincent et al. (2011) Dziruli
Avdeev & Niemi (2011)
This study
AFT
Kral & Gurbanov (1996)
Vincent et al. (2011)
Vincent et al. (2011) Dziruli
Avdeev & Niemi (2011)
This study
AHe
This study
Sample within 10 km of a Cenozoic magmatic center
Polyak et al. (2000, 2011) He isotopes
Thermal overprinting

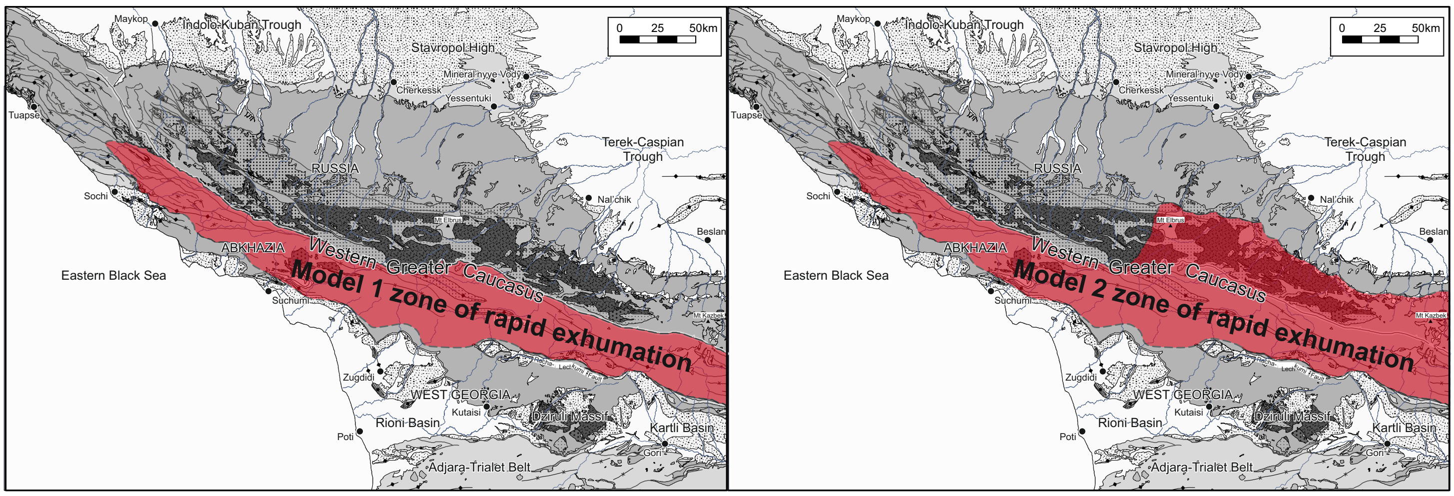

Maykop
Indolo-Kuban Trough
Stavropol High
0 25 50km
Mineral'nyye Vody
Cherkessk
Yessentuki
Tuapse
Terek-Caspian
Trough
RUSSIA
Sochi
Nal'chik
Beslan
Mt Elbrus
ABKHAZIA
Western Greater Caucasus
Eastern Black Sea
Model 1 zone of rapid exhumation
Suchumi
Zugdidi
WEST GEORGIA
Kutaisi
Dzirula Massif
Rioni Basin
Kartli Basin
Poti
Gori
Adjara-Trialet Belt
Maykop
Indolo-Kuban Trough
Stavropol High
0 25 50km
Mineral'nyye Vody
Cherkessk
Yessentuki
Tuapse
Terek-Caspian
Trough
RUSSIA
Sochi
Nal'chik
Beslan
Mt Elbrus
ABKHAZIA
Western Greater Caucasus
Eastern Black Sea
Model 2 zone of rapid exhumation
Suchumi
Mt Kazbek
Zugdidi
WEST GEORGIA
Kutaisi
Dzirula Massif
Rioni Basin
Kartli Basin
Poti
Gori
Adjara-Trialet Belt

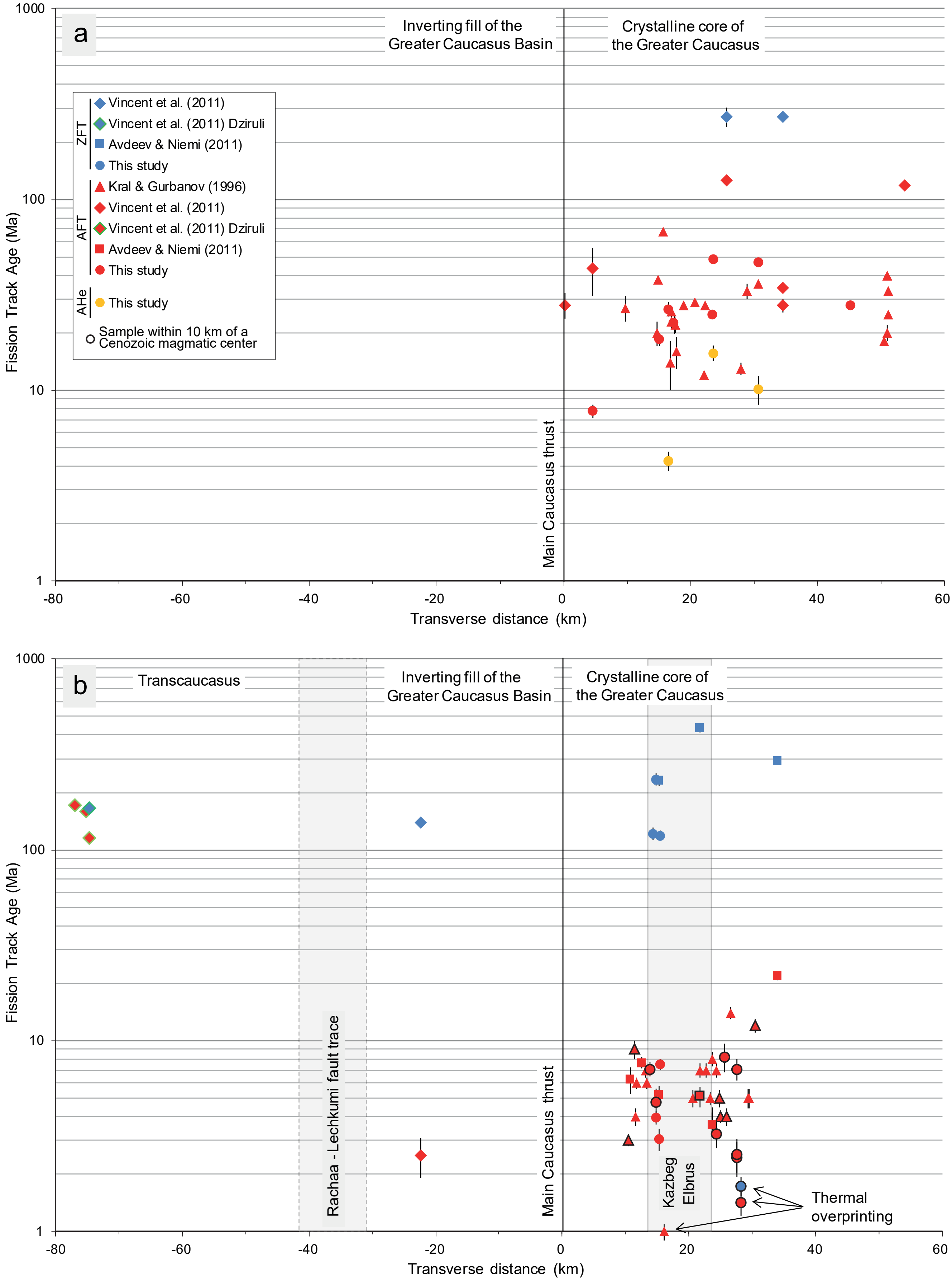
a
Inverting fill of the
Greater Caucasus Basin
Crystalline core of
the Greater Caucasus
ZFT
Vincent et al. (2011)
Vincent et al. (2011) Dziruli
Avdeev & Niemi (2011)
This study
AFT
Kral & Gurbanov (1996)
Vincent et al. (2011)
Vincent et al. (2011) Dziruli
Avdeev & Niemi (2011)
This study
AHe
This study
Sample within 10 km of a Cenozoic magmatic center
Main Caucasus thrust
Fission Track Age (Ma)
1000
100
10
1
-80
-60
-40
-20
0
20
40
60
Transverse distance (km)
b
Transcaucasus
Inverting fill of the
Greater Caucasus Basin
Crystalline core of
the Greater Caucasus
Rachaa -Lechkumi fault trace
Main Caucasus thrust
Kazbeg
Elbrus
Thermal
overprinting
Fission Track Age (Ma)
1000
100
10
1
-80
-60
-40
-20
0
20
40
60
Transverse distance (km)

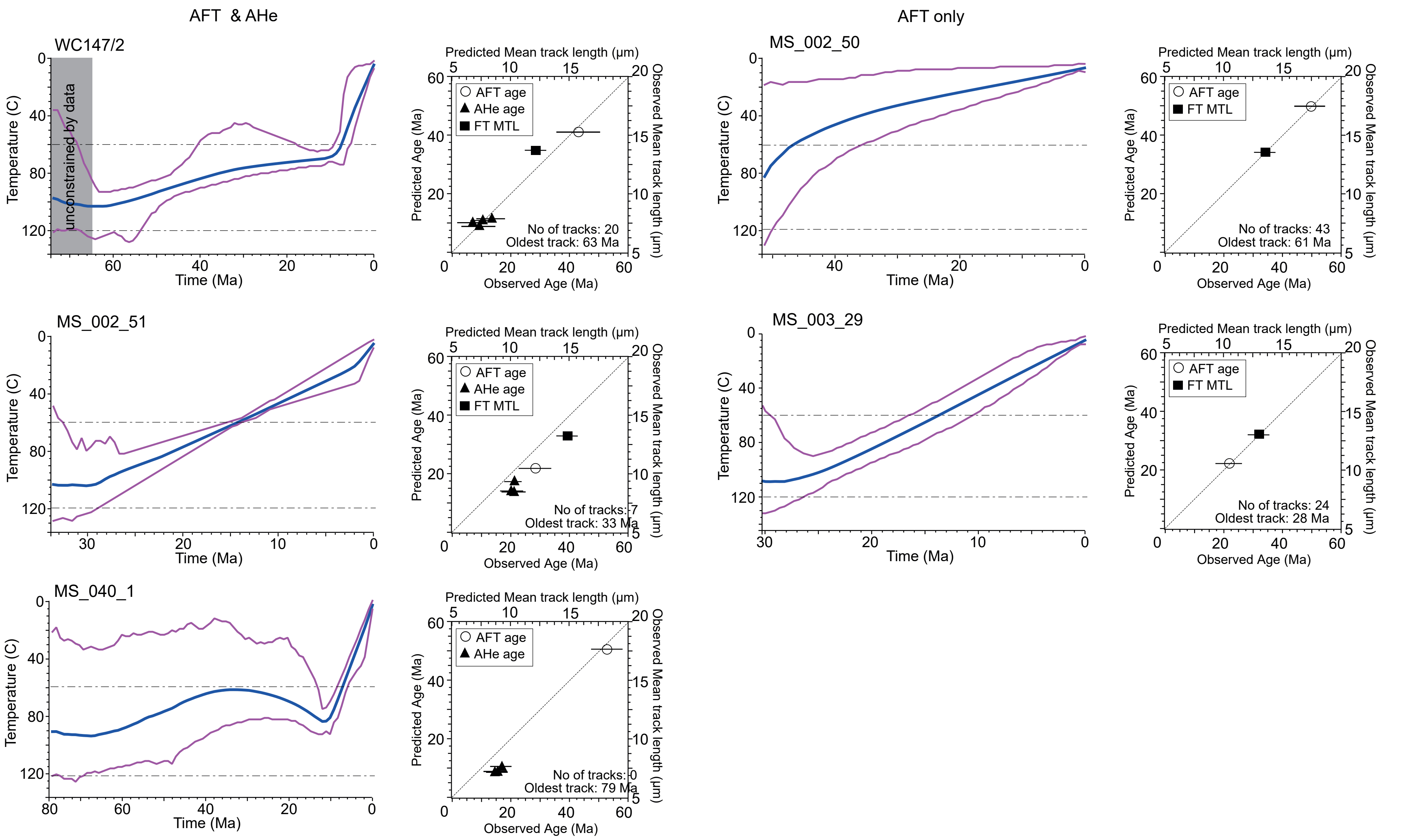
AFT & AHe
AFT only
WC147/2
unconstrained by data
Temperature (C)
Time (Ma)
Predicted Mean track length (µm)
Observed Mean track length (µm)
Predicted Age (Ma)
Observed Age (Ma)
AFT age
AHe age
FT MTL
No of tracks: 20
Oldest track: 63 Ma
MS_002_50
No of tracks: 43
Oldest track: 61 Ma
MS_002_51
No of tracks: 7
Oldest track: 33 Ma
MS_003_29
No of tracks: 24
Oldest track: 28 Ma
MS_040_1
No of tracks: 0
Oldest track: 79 Ma

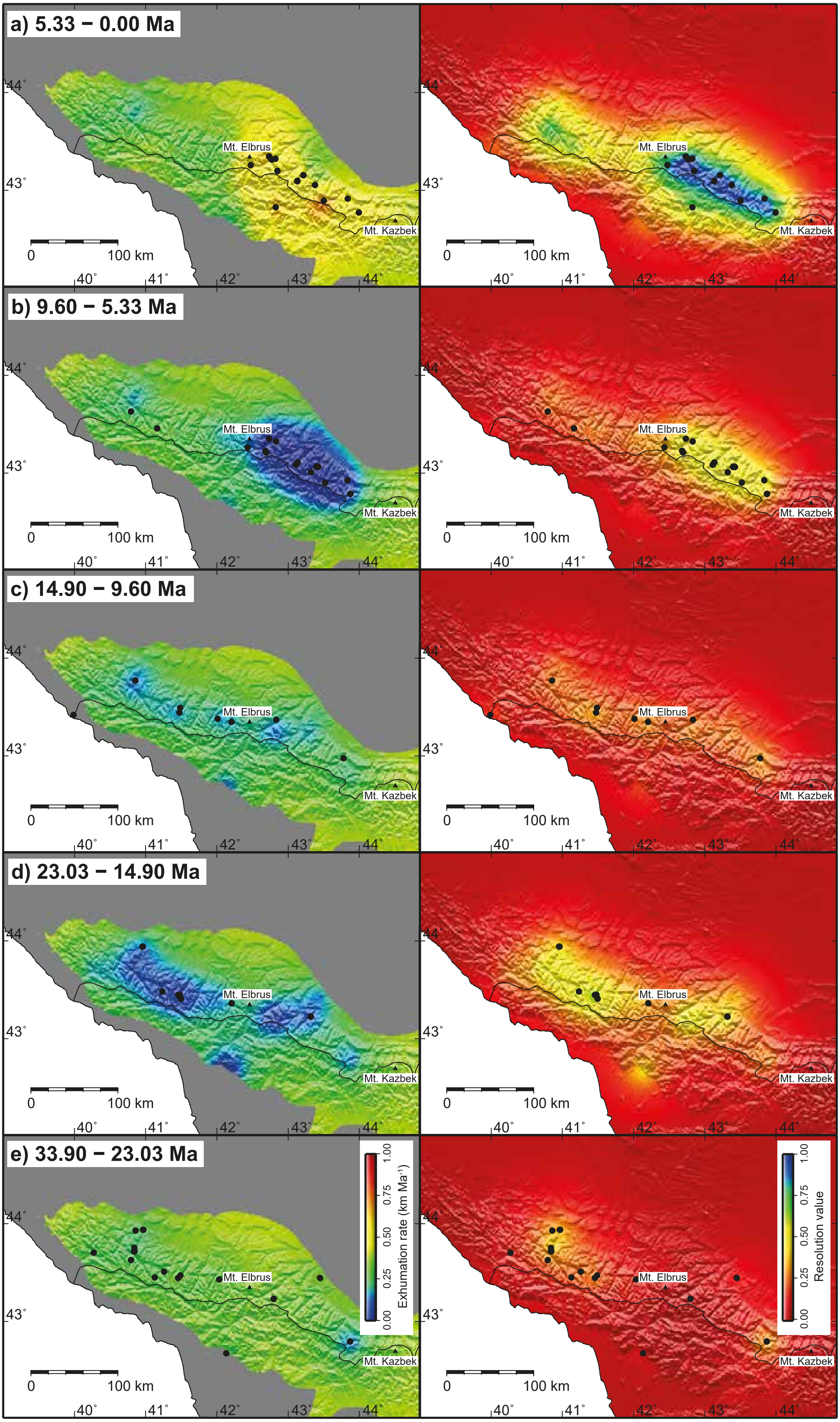

a) 5.33 – 0.00 Ma
b) 9.60 – 5.33 Ma
c) 14.90 – 9.60 Ma
d) 23.03 – 14.90 Ma
e) 33.90 – 23.03 Ma
Mt. Elbrus
Mt. Kazbek
0
100 km
44°
43°
40°
41°
42°
43°
44°
Exhumation rate (km Ma-1)
0.00
0.25
0.50
0.75
1.00
Resolution value

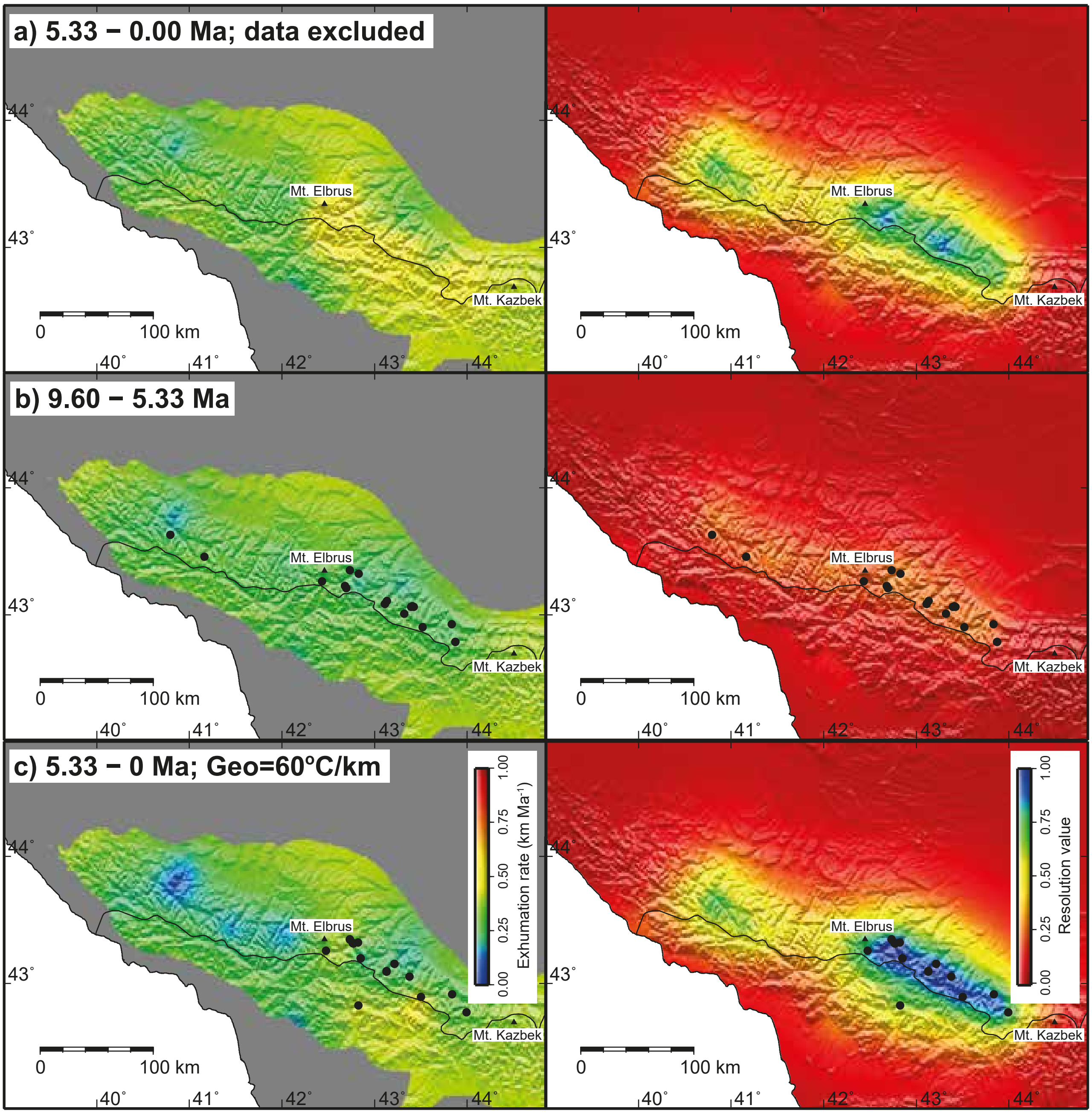

a) 5.33 − 0.00 Ma; data excluded
b) 9.60 − 5.33 Ma
c) 5.33 − 0 Ma; Geo=60ºC/km
Mt. Elbrus
Mt. Kazbek
0
100 km
40˚
41˚
42˚
43˚
44˚
Exhumation rate (km Ma-1)
0.00
0.25
0.50
0.75
1.00
Resolution value

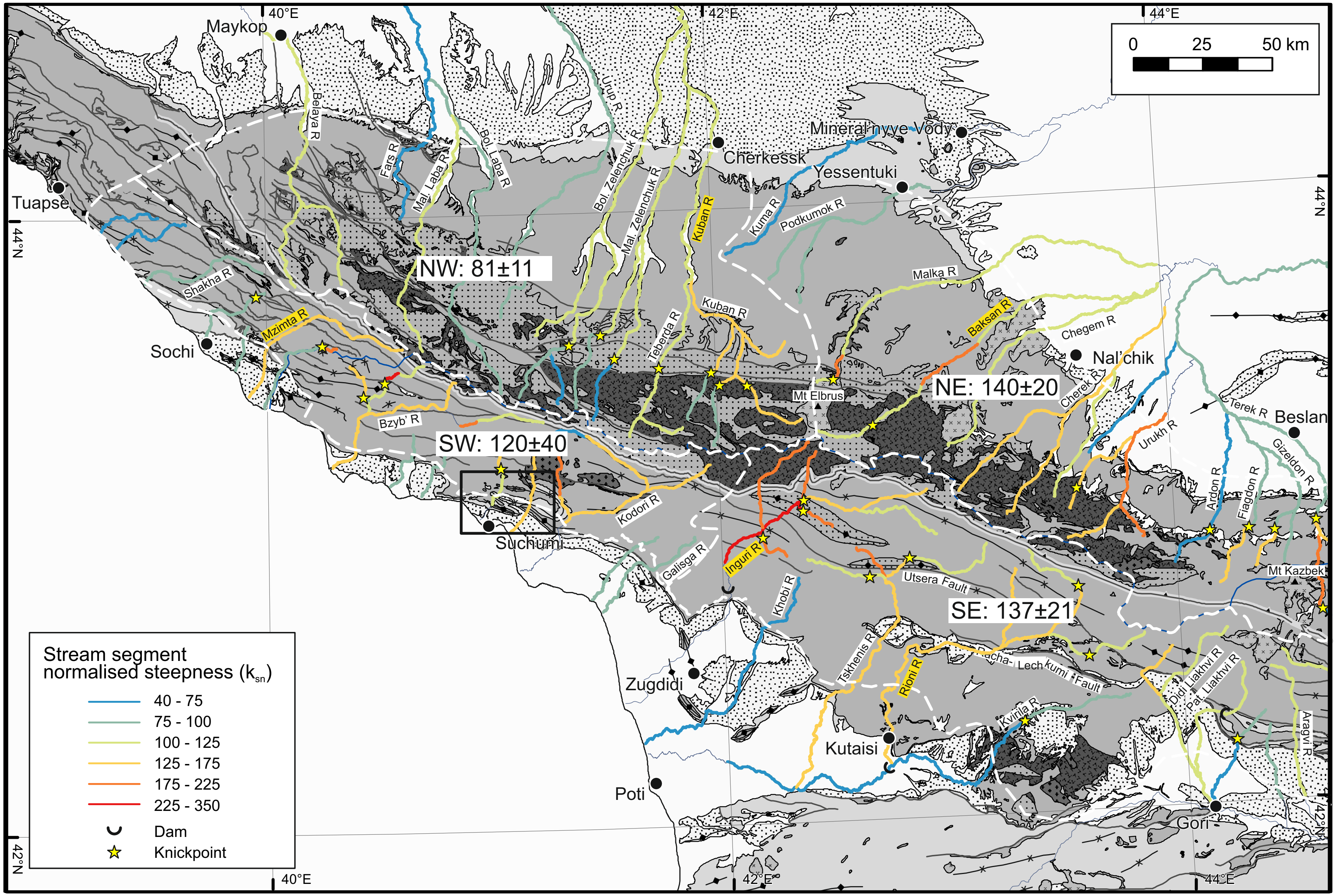

Stream segment normalised steepness (k_{sn})
40 - 75
75 - 100
100 - 125
125 - 175
175 - 225
225 - 350
Dam
Knickpoint
0 25 50 km
NW: 81±11
NE: 140±20
SW: 120±40
SE: 137±21
Maykop
Tuapse
Sochi
Suchumi
Zugdidi
Poti
Kutaisi
Gori
Cherkessk
Mineral'nyye Vody
Yessentuki
Nal'chik
Beslan
Mt Elbrus
Mt Kazbek
Belaya R
Fars R
Mal. Laba R
Bol. Laba R
Urup R
Bol. Zelenchuk R
Mal. Zelenchuk R
Kuban R
Kuma R
Podkumok R
Malka R
Baksan R
Chegem R
Cherek R
Urukh R
Terek R
Gizeldon R
Ardon R
Fiagdon R
Shakha R
Mzimta R
Bzyb' R
Kodori R
Teberda R
Galisga R
Ingur R
Khobi R
Tskhenis R
Rioni R
Kvirila R
Didi Liakhvi R
Pat. Liakhvi R
Aragvi R
Utsera Fault
Racha-Lechkumi Fault
40°E
42°E
44°E
44°N
42°N

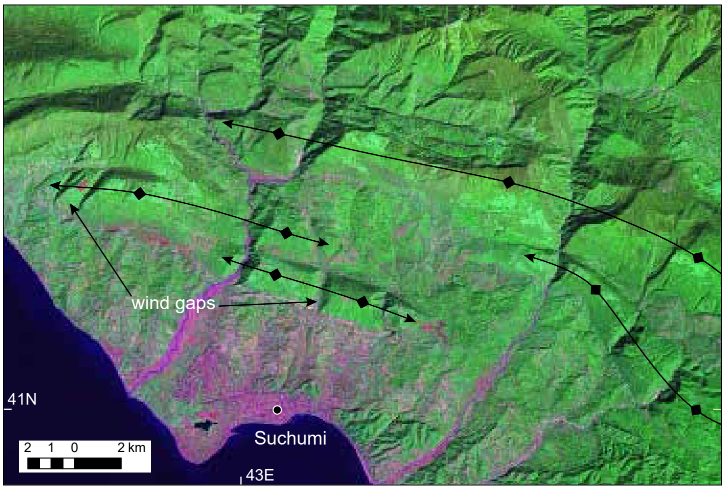
wind gaps
41N
Suchumi
2 1 0 2 km
43E